NUMERICAL ANALYSIS OF FLOW CHARACTERISTICS NEAR NEIGHBOURING VEGETATION PATCHES OF DIFFERENT DENSITIES

Master thesis
Department of Water Engineering & Management
Faculty of Engineering Technology

Maartje Geurts
July 2022

Graduation committee:
University of Twente
Dr.ir. B.W. Borsje
Dr. V. Kitsikoudis
Dr.ir. A. Bomers

UNIVERSITY OF TWENTE.

Preface

This thesis is the last step to completing my master Civil Engineering and Management at the University of Twente. This thesis was carried out at the Water Engineering and Management department, which allowed me to explore interests that I did not even know I had. I discovered that I quite like constructing a model, especially when it also works and provides interesting results. I would like to thank my daily supervisors, Vasileios Kitsikoudis and Anouk Bomers, for the weekly meetings, new insights and good, alternative ideas when not everything went according to plan. Thank you for always being open to my many questions and doubts, and expanding my knowledge on both the physical processes as well as the modelling aspects of this research. I would also like to thank Bas Borsje, head of the graduation committee, for his sharp questions that challenged me to think further, and for providing his insights in how to improve this research.

Furthermore I would like to thank my family, friends and boyfriend for their unconditional support. Not only during the last six months but also the previous years of my student life. I have been on amazing adventures these last couple of years, and although Covid-19 messed up some of my plans, there were enough creative people around me to still make it work. Thank you for being there with me and filling my days with good food, exiting activities and great memories.

Regarding this research, I would like to give a special thanks to my boyfriend and my dad, for patiently proofreading 40 pages of text about a subject they previously did not understand. And of course to my studybuddies, for spending a lot of time with me these past few months and always offering support in any shape or form.

I hope you will enjoy reading this report!

Maartje Geurts
July 2022

Summary

River vegetation provides a lot of benefits to its environment, however there are also some negative effects related to this vegetation. Some of these benefits are improving the water quality and providing a habitat, a negative effect is the addition of drag which could lead to a rise in water levels. In order to manage river vegetation it is important to gain a better understanding of the effect it has on the flow. A lot of research has focused on either a single vegetation patch or two vegetation patches in order to investigate the flow processes generated by the presence of a vegetation patch and the interaction between multiple patches. Not much research has gone into understanding the processes surrounding two patches with different densities, and when this is considered, the location between the patches is not varied to study the additional influence of that aspect. In order to expand the knowledge on river vegetation, it is necessary to gain a better understanding of the behaviour around vegetation patches of different densities with varying interpatch distances. This led to the objective of this research: to study the effect of vegetation patches with different densities on the flow velocity distribution and sediment deposition.

In order to do this, the first step was to construct a numerical model with the CFD code FLUENT®. Several different model settings and turbulence closure models were tested and compared against validation data of a single vegetation patch with a solid volume fraction of 3%. Two aspects were of main interest: the length of the steady wake region and the simulated flow velocities on the centerline behind the patch. A circular patch with 37 stems and a RNG $k-\epsilon$ turbulence closure model with standard wall functions corresponded best with the validation data. The difference between the simulated steady wake length and the steady wake length of the validation patch was 13%. The maximum difference between the simulated centerline velocities and the measured centerline velocities of the validation data was 11%.

It was found that changing the density of an upstream patch does not have a significant effect on the wake velocity of the downstream patch. The turbulence levels in the wake of the downstream patch were affected and increased for denser upstream patches. Different densities for the downstream patch had a much larger effect on the wake of the upstream patch compared to the effect of an upstream patch with different densities. A denser downstream patch resulted in a shorter steady wake length and higher minimum velocities behind the upstream patch. Turbulence levels were also higher and a Turbulent Kinetic Energy (TKE) peak was seen further upstream for a denser downstream patch compared to a sparser patch. When the patches were placed further apart in the longitudinal direction ($6D$), the steady wake length behind the upstream patch became longer and the TKE at the end of the steady wake region was higher than for patches placed closer together. When the patches were placed further apart in the transverse direction ($2.5D$), it was found that the upstream wake recovered quicker to the undisturbed upstream velocity.

The last step was to evaluate the sediment deposition. Two methods were used to analyse this. The first method was the velocity and TKE method, in which a threshold velocity and threshold TKE value were selected. If the measured values are below the threshold values, sediment deposition takes place.With this method it was found that the location of the patches does not matter, only the amount of flow blockage they represent combined. A patch combination with sparser patches resulted in a larger area of enhanced sediment deposition. Another method was the velocity threshold method. For this method only a threshold velocity was chosen, below which sediment deposition takes place. This method concluded that patch combinations which presented a larger flow blockage will result in more area of enhanced sediment deposition and thus an increase in potential new vegetation growth. Both methods did find that the most significant location of enhanced sediment deposition occurred behind the patch, extending from the steady wake region. Both methods also did not report the presence of a secondary deposition zone.

In conclusion, the density of a neighbouring patch placed downstream of another patch had a significant effect on the flow velocities and turbulence levels in the wake of the upstream patch. Depending on the density and location, these effects were increased or reduced, but always present

for the chosen interpatch distances. The density of a neighbouring patch placed upstream of another patch had no significant effect on the wake of the other patch. In terms of sediment deposition and vegetation growth, the most significant changes in the areas of enhanced sediment deposition were related to different patch densities and not as much to the location of the patches. Both methods found enhanced sediment deposition behind each patch, meaning that there is a possibility for longitudinal expansion of the patches, however patch merger is unlikely according to the model results.

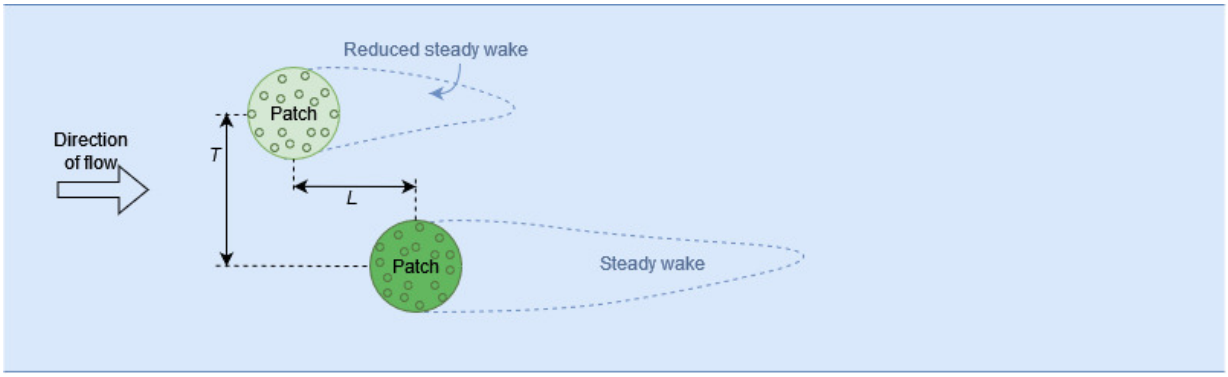

Figure 0.1: Top view of two vegetation patches with different densities in a flow domain. The blue striped line denotes the steady wake region behind each patch and how it is affected by the presence of a neighbouring patch. T represents the transverse distance between the centers of the two patches and L the longitudinal distance between the centers of both patches.

Contents

List of Figures

List of Tables

1 Introduction

River vegetation provides a lot of benefits to the environment. By trapping sediment, vegetation is responsible for reducing turbidity (Jones et al., 2012), it provides habitat for aquatic animals (Kemp et al., 2000) and it has a positive effect on the water quality by taking up nutrients, such as ammonium (Cornacchia et al., 2019). With all the services that vegetation provides, such as regulation of oxygen and carbon dioxide levels and erosion control, Costanza et al. (1996) concluded that aquatic plants are actually highly beneficial in terms of financial costs. Preserving river vegetation is thus of great importance, although there are some downsides. Vegetation is responsible for drag, which reduces the flow velocity. In order to satisfy continuity of the flow, the flow depth increases which means that the water level will rise. In extreme occasions, this could lead to river flooding (Nepf, 2012). Therefore a better understanding of the behaviour of flow around aquatic vegetation is required.

1.1 Background

Flow around a single vegetation patch is often characterized by the steady wake region that is formed behind the patch, as shown in Figure 1.1 (Chen et al., 2012). This steady wake is created by bleed flow, a portion of the approaching flow that is forced through the vegetation patch (Nepf, 2012). A von Kármán vortex street that would normally appear right behind a solid obstacle is shifted further downstream due to the bleed flow (Chen et al., 2012). Within the steady wake region, the velocity and turbulence are low which gives the opportunity for sediment to settle down. As well as sediment, plant propagules, or spores, are transported by the flow and once settled, they can grow to become new vegetation patches (Gurnell, 2014). The portion of the flow that goes around the vegetation patch accelerates, which in some cases could lead to erosion. As this accelerated flow starts to mix with the wake region, a von Kármán vortex street will start to form. From this point on, the flow velocity in the wake region increases and starts to recover towards its upstream value (de Lima et al., 2015). These previous processes are portrayed by the broad, grey lines in figure 1.1. In figure 1.1, two regions of elevated turbulence are indicated. The first is the stem-scale turbulence which is the turbulence generated by each stem, and peaks right behind the most downstream stem. The second peak is the patch-scale turbulence and generated with the formation of the von Kármán vortex street. This peaks at distance L_w from the patch, as seen in figure 1.1 (Chen et al., 2012).

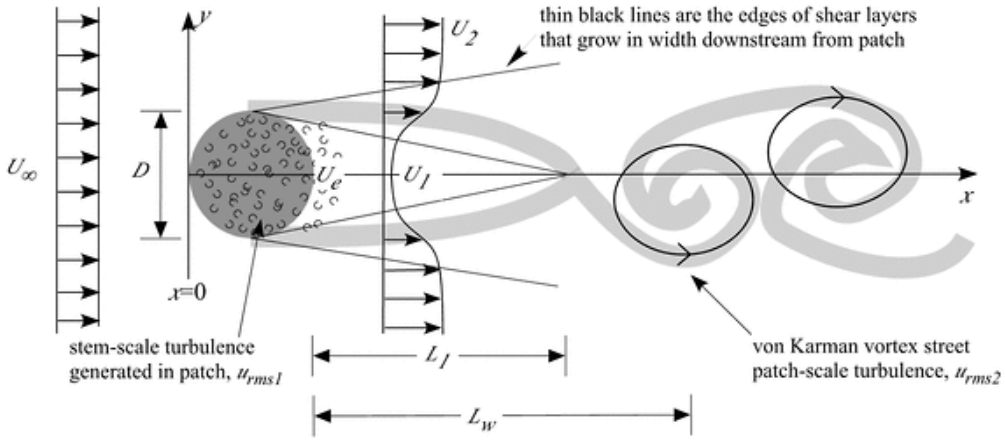

Figure 1.1: Top view of the flow around a single vegetation patch, in which U_∞ is the upstream velocity, U_1 is the flow velocity in the steady wake region, U_2 is the velocity of the diverted flow, L_1 is the distance from the patch at which the von Kármán vortex street starts and L_w is the distance from the patch to the peak of the patch-scale turbulence (Chen et al., 2012)

The development and length of the steady wake region are dependent on the patch density (Zong and Nepf, 2011). A sparser patch allows for more bleed flow, which results in a higher velocity in the steady wake region. For a denser patch, a larger portion of the flow diverts around the patch, resulting in less bleed flow and thus a lower flow velocity in the steady wake region. Due to this, the velocity gradient between the wake velocity and the velocity of the flow around the patch is steeper for a denser patch, and leads to an increase of turbulence (Zong and Nepf, 2012).

When flow behaviour around river vegetation is investigated in an experimental setup, researchers often replace vegetation patches with rigid cylinders of a wooden or steel material (Meire et al. 2014; Kitsikoudis et al. 2020). Other researches have made computational models in which the stems were replaced with rigid cylinders (de Lima et al., 2015). This simplification still bears a resemblance to aquatic plants such as *Spartina alterniflora*, but leaves out many of the uncertainties associated with the use of real vegetation, such as oscillation of the stems or additional drag formed by leaves (Schnauder and Moggridge, 2009). These simplifications also result in shorter computing times for computational models. Therefore such simplifications are useful, however one must keep in mind that the results could differ from reality. The density of such simplified patches can be described in different ways. One way is to multiply the amount of stems by the diameter of each stem, as shown in Equation (1) (Meire et al., 2014). Two other methods that are often used are calculating the flow-blockage factor (Eq. 2) and the solid volume fraction (Eq. 3) (Chen et al., 2012).

$$a = nd \tag{1}$$

$$blockage = C_d a D \tag{2}$$

$$\phi = \frac{\pi d^2}{4} \cdot n \tag{3}$$

Where:

- a: is the patch density [1/m]
- n: is the amount of stems per area [1/m^2]
- d: is the mean stem diameter [m]
- C_d: is the stem drag coefficient [-]
- D: is the patch diameter [m]
- ϕ: is the solid volume fraction [-]

When two (simplified) vegetation patches are used for research, they can either be placed in a side-by-side or in a staggered manner, as shown in figure 1.2a and 1.2b. If the patches are placed close enough to each other, an interaction could take place (de Lima et al., 2015). On the centerline between two patches placed side-by-side, a jet stream can occur, which leads to enhanced velocities between the patches. Further downstream, the centerline velocity will reach a minimum when the two wakes of the patches merge (Meire et al., 2014). The diminished velocities caused by the wake merger allow for sediment to settle and could eventually lead to new vegetation growth downstream of the two patches. This new vegetation reduces the velocity between the two original patches, which allows for circumstances in which even more vegetation can grow. These processes could then lead to patch merger, as Yamasaki et al. (2021) found in a flume setup. For patches in a staggered position, it was found that the steady wake length of the upstream patch was shortened by the presence of a downstream patch. This shortening of the steady wake was caused by the flow diverting around the downstream patch. The steady wake length behind the upstream patch was even shorter for a denser downstream patch, and became longer and almost represented a single

patch again for a sparser downstream patch (Kitsikoudis et al., 2020). Patch merger is not as easily achieved for staggered patches, but a positive feedback is considered when the total vegetation growth due to patch interaction is larger than the vegetation growth behind two individual patches. If the patches are placed close enough together on the cross-section ($T<1.3D$ for fine sediment and $T<1.5D$ for larger sediment), such a positive feedback can occur for various longitudinal distances L (de Lima et al., 2015).

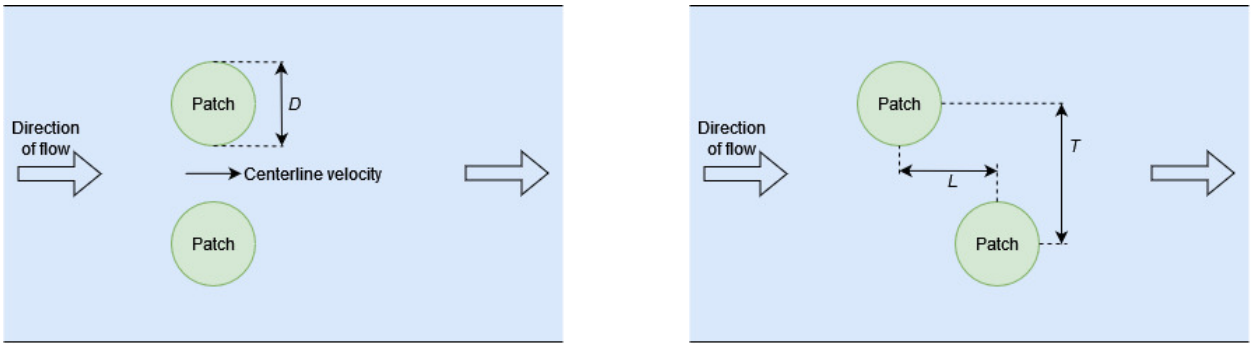

(a) (b)

Figure 1.2: Top view of vegetation patches placed side-by-side (a) and set up in a staggered position (b). D is the patch diameter, L is the longitudinal distance between the patches from center to center and T is the transverse distance between the patches from center to center.

Researchers such as de Lima et al. (2015) and Yamasaki et al. (2019) use numerical models for their simulations. One of the most commonly applied methods to analyze fluid dynamics is with Reynolds Averaged Navier Stokes (RANS) equations. These RANS equations are derived from the Navier-Stokes equations, which are split into the time-averaged solution and velocity fluctuations. The problem is that these equations cannot be closed due to the remaining fluctuations. In order to solve the latter, a turbulence closure model is necessary (Jones et al., 2016). There are several turbulence closure models, such as the $k-\epsilon$ model, the $k-\omega$ model and the $k-\omega$ SST model with each their own qualities. These models and equations will be explained in more detail in Section 2.

1.2 State of the art

With the presence of a vegetation patch, positive and negative feedback loops can occur. A positive feedback loop can occur in the wake of the vegetation patch (Vandenbruwaene et al., 2011). As mentioned, in this region, the flow velocity and turbulence are very low due to the drag that vegetation applies on the flow. This could lead to the settlement and growth of new vegetation (Gurnell, 2014). This new vegetation results in more drag and more low flow velocities, which again promotes the growth of new vegetation.

A negative feedback loop can occur as the flow is forced around a vegetation patch, increasing the flow velocity. These increased velocities could lead to erosion of the bed, which inhibits the growth of new vegetation (Bouma et al., 2007). To reduce or manage negative effects, and to increase development and restoration of the vegetation, it is important to gain more knowledge on the way that a river is affected by vegetation (Kondziolka and Nepf, 2014). A way to start is by investigating the flow around either one vegetation patch or multiple vegetation patches, by using field or flume experiments, or constructing a computational model.

A lot of research has already been done about the flow structure inside and around a single vegetation patch. However, only a few researchers have looked into the interaction that occurs when two vegetation patches are placed close enough to each other. Meire et al. (2014) ran a flume experiment in which two simplified vegetation patches were placed side-by-side. They investigated

the influence of different stem densities and different gap widths between the patches on the patterns of flow and deposition. In particular they looked at the velocity increase and decrease on the centerline and how the wakes of the patches interact. The patches they used have a solid volume fraction of ϕ=3.3, 3.7, 10 and 11%. They found that the steady wake length and wake velocity were not affected by a neighbouring patch, unless the two patches were placed right next to each other. In that case they start to resemble a larger, single patch. For their experiments, the maximum gap between the centers of the two patches was $2D$, which in all cases resulted in wake merger downstream of the patches. This wake merger occurred at a shorter distance for the denser patches, because they generate a larger level of turbulence. Turbulence enhances the mixing of the flow towards flow recovery, and with a higher level of turbulence this mixing is faster. Furthermore, they found three zones of enhanced deposition: directly upstream and directly downstream of each patch, and further downstream on the centerline between the two patches where the wakes merge.

de Lima et al. (2015) and Yamasaki et al. (2019) experimented with multiple vegetation patches both placed in side-by-side manner and a staggered manner. They used FLUENT® modelling code in two-dimensional depth-averaged (2DH), with RANS equations and a $k-\epsilon$ turbulence closure model. A 2DH model is a 2D model in which the horizontal plane is studied. The use of the 2D model in the horizontal plane was justified, since it was concluded that for emergent vegetation, the most prominent flow patterns will happen in the horizontal plane. They validated this model with the experimental research performed by Zong and Nepf (2012) by constructing a single vegetation patch with a diameter of 22 cm and a solid volume fraction of 0.03. The mean velocity on the centerline upstream and downstream of the patch, and the transverse profile of the longitudinal velocity measured along a line at $y = D/2$ are both compared to the experimental data of Zong and Nepf (2012), and a maximum difference of 6% between both data sets was found. For the simulations 46 variations of distances for T and L were performed. The patches de Lima et al. (2015) used had a solid volume fraction of ϕ=10%. For staggered patches they found that if the longitudinal distance L between the patches was smaller than $6D$, an interaction between the two patches occurred. The largest transverse distance T that was experimented with was $3D$, which always resulted in an interaction. In terms of potential sedimentation, which was based on the flow velocity, they found that a positive feedback loop always occurred for $T<1.3D$, resulting in enhanced sedimentation compared to two individual patches.

Yamasaki et al. (2019) also constructed a horizontal 2D model with RANS equations and a $k-\epsilon$ turbulence closure model. Instead of selecting a density for a single vegetation patch, they selected two initial blockage factors to portray the coverage of the channel: 0.3% and 3%. They ran simulations with set ups of multiple vegetation patches and initial blockage factors to investigate how vegetation can grow over time, which is based on the flow velocity. They found that a positive feedback between two patches did have an effect on the initial growth of vegetation, as it speeds up the spreading of new vegetation. However, for the final vegetation coverage, it did not matter how close the patches were at the initial stage and whether or not positive feedback loops took place, the final vegetation coverage would always be the same.

1.3 Problem definition

All the research mentioned in Section 1.2 focused on patches with the same density, such as two sparse vegetation patches or two dense vegetation patches. However they overlook or ignore the fact that there could be a difference in density between the two patches. In reality, it is highly unlikely that two patches of the same density will be next to each other (Kitsikoudis et al., 2020). Cornacchia et al. (2019) do make this distinction, however their focus is more on the implications for the ammonium uptake rate, instead of the implications of different densities on the flow distribution. Kitsikoudis et al. (2020) performed flume experiments in which the densities of the two vegetation patches were different from each other. For their experiments, they used their own distribution of three different types of densities: sparse, medium and dense. The solid volume fraction was used

to classify these patches, for which the sparse patch was equal to ϕ=0.06, the medium patch was equal to ϕ=0.11 and the dense patch gave ϕ=0.19. The patches were placed either side-by-side or in a staggered manner, as is shown in Figures 1.2a and 1.2b. The longitudinal distances that were tested were either L=0D or 3.5D and the transverse distance was chosen was T=1.5D. They found that the wakes of patches placed side-by-side are not significantly affected by varying densities of the two patches. However, the wakes of the patches are influenced by the different densities when the patches are placed in a staggered manner. They were however limited to the time it takes to set up and perform a flume experiment, and to the available materials and flume size in order to run tests. Therefore it is necessary to develop a numerical model that investigates the flow around vegetation patches of different densities, in which it is possible to experiment with the interpatch distance, the patch densities, the patch diameter and the approaching velocity to get insight in how these factors have an effect on the flow. Additionally, with a numerical model it is possible to evaluate the flow properties over the whole domain, instead of only the limited amount of areas where measuring equipment is placed.

1.4 Objective and research questions

This research will build further on the research by de Lima et al. (2015) where they look at the influence of two vegetation patches on the flow velocity and sediment deposition. In order to do this a numerical 2DH model will be constructed. The objective is to investigate the influence of two vegetation patches with each having a different density. The research question and sub questions are then as follows:

What is the effect of vegetation patches with different densities on the flow velocity distribution and sediment deposition?

1. Which model settings and turbulence closure model are the most successful in achieving realistic values for the flow velocity and turbulent kinetic energy compared to results from literature?
2. What is the effect of changing the density of each patch and altering the interpatch distance on the flow recovery pattern and length for the whole horizontal domain?
3. How is sediment deposition and vegetation growth affected by changing the density for each patch and the interpatch distance?

2 Theoretical framework

In order to investigate the influence of different patch densities, a numerical model is used. Computational Fluid Dynamics (CFD) is a numerical method and a helpful tool to investigate the flow of water in detail. With CFD modelling, it is possible to analyse complex real-life scenarios, such as the flow in a river (Giraldo, 2021). In order to simulate the turbulence that is present in a river, a CFD model that employs the Reynolds Averaged Navier Stokes (RANS) equations is selected. As mentioned in section 1.1, RANS models produce mean velocities that are relatively accurate compared to the small computation times. When turbulence and vortices are of special interest, more detailed models such as the Large Eddy Simulation (LES) model are a better option. However, the use of these models is about 10 to 100 times as computationally costly compared to the use of RANS models (Fröhlich and von Terzi, 2008). Due to time limitations and an interest in the large-scale turbulence processes and average flow velocities, a RANS model is selected for this research.

2.1 Navier-Stokes equations

The Navier-Stokes equations are used to express any type of fluid flow. Since they can describe any fluid, there are many different scales involved within the equations. The Navier-Stokes equations for an incompressible fluid are shown in vector form in Equation (4), obtained from Kitsikoudis and Huthoff (2021). Term i describes the local acceleration in a fluid element, term ii describes the momentum flux through a fluid element, term iii is the gravity force, term iv is the pressure on a fluid element and term v describes the viscous forces for a fluid element (Kitsikoudis and Huthoff, 2021).

$$\underbrace{\frac{\partial \vec{v}}{\partial t}}_{\text{(i)}} + \underbrace{\vec{v} \cdot \nabla \vec{v}}_{\text{(ii)}} = \underbrace{\vec{g}}_{\text{(iii)}} - \underbrace{\frac{1}{\rho} \nabla P}_{\text{(iv)}} + \underbrace{\nu_m \nabla^2 \vec{v}}_{\text{(v)}} \tag{4}$$

Solving the Navier-Stokes equations numerically presents its own challenges, since a very fine mesh is needed for a relatively large computing field. Moreover, with the many non-linear equations, the flows become chaotic for high Reynolds numbers (Kitsikoudis and Huthoff, 2021). In order to solve the equations numerically, adaptations have been made, leading to the Reynolds Averaged Navier Stokes (RANS) equations. First, Reynolds averaging is done by taking the Reynolds decomposition equation (Eq. 5) and applying it to the Navier-Stokes equation above. The result is shown in vector notation in Equation (6). The term $\boldsymbol{R}$ in Equation (6) stands for the Reynolds stress tensor, which is also written as τ_{ij} in Equation (7) (Kitsikoudis and Huthoff, 2021). In order to close the RANS equations, all the terms need to be described as mean variables (Jones et al., 2016). A next step is to implement the Boussinesq approximation, which is shown in Equation (8). The Turbulent Kinetic Energy (TKE), k, for a 2D flow is given in Equation (9) (Yamasaki et al., 2019). Since fluctuations will remain, additional models are needed to close the RANS equations. These will be discussed in Section 2.2.

$$u = \bar{u} + u' \tag{5}$$

$$\frac{\partial \vec{v}}{\partial t} + \vec{v} \cdot \nabla \vec{v} = \vec{g} - \frac{1}{\rho} \nabla \bar{P} + \nu_m \nabla^2 \vec{v} + \frac{1}{\rho} \nabla \cdot R \tag{6}$$

$$\tau_{ij} = -\rho \overline{u_i' u_j'} \tag{7}$$

$$-\rho \overline{u_i' u_j'} = \mu_t \left(\frac{\partial u_i}{\partial x_j} + \frac{\partial u_j}{\partial x_i} \right) - \frac{2}{3} \rho k \delta_{ij} \tag{8}$$

$$k = \frac{1}{2}(\bar{u_1'^2} + \bar{u_2'^2}) \tag{9}$$

Where:

- u: flow velocity in the x direction [m/s]
- $\bar{u}$: mean flow velocity in the x direction [m/s]
- u': deviation from the mean velocity in the x direction [m/s]
- ρ: density of the fluid [kg/m^3]
- P: pressure [Pa]
- ν_m: kinematic viscosity of the fluid [m^2/s]
- τ_{ij}: Reynolds stress tensor [N/m^2]
- μ_t: eddy viscosity [Ns/m^2]
- δ_{ij}: Kronecker delta [-]
- g: gravitational acceleration [m/s^2]
- k: Turbulent Kinetic Energy [m^2/s^2]

2.2 Turbulence closure models

Apart from the $k-\epsilon$ turbulence closure model, there are also the $k-\omega$ and the $k-\omega$ SST turbulence closure models that are used in CFD modelling and are developed to predict the eddy viscosity and close the RANS equations (Durbin, 2004).

The $k-\epsilon$ model is sufficiently accurate at calculating flows in free-stream conditions and adequate for calculating flows near walls for small pressure gradients (Bardina et al., 1997). The $k-\omega$ model is very useful for calculating the flow near walls, but is unreliable for free-stream conditions. To solve this, the $k-\omega$ SST model was developed which combines the $k-\omega$ model with the $k-\epsilon$ model. This combination is made by inserting a blending function that enables the transition between the two models around the middle of the boundary layer. $k-\omega$ will then be applied close to the wall and $k-\epsilon$ will be applied to the rest of the flow (Durbin, 2004).

From the standard $k-\epsilon$ model, several improvements have been made, resulting in the realizable $k-\epsilon$ model and the RNG $k-\epsilon$ model. The realizable $k-\epsilon$ model is known for its improved results for layer mixing, boundary layers and flow separation. The RNG $k-\epsilon$ model has improved results for the recirculation length when flow separation occurs (Ye et al., 2021).

2.3 Wall functions and y^+ value

The boundary layer that exists next to a wall consists of four parts, which are the viscous sublayer, the buffer layer, the log-law region and the outer layer (ANSYS Inc., 2014). These layers are shown in figure 2.1. To describe the velocity and turbulent kinetic energy in these regions as accurately as possible, the y^+ value plays a large role. y^+ is a value that is often used to describe the height of the first grid cell next to the wall, and is also influenced by the properties of the fluid and the local flow velocity, as can be seen in Equations (10) and (11) (ANSYS Inc., 2014).

$$y^+ = \frac{\rho U_\tau y}{\nu_m} \tag{10}$$

$$U_\tau = \sqrt{\frac{\tau_w}{\rho}} \tag{11}$$

Where:

- y^+: wall distance [-]
- U_τ: wall shear stress velocity [m/s]
- y: distance to nearest wall [m]
- τ_w: wall shear stress [Pa]

Wall functions in CFD modelling are used to compute the physics that occur in the boundary layers. As mentioned in the previous paragraph, especially the $k-\epsilon$ model can have issues with providing accurate results close to a wall, which can be solved by applying wall functions. In general, wall functions for the $k-\epsilon$ model require a y^+ between 30 and 300 (ANSYS Inc., 2014). This ensures that the center of the cell closest to the wall is located in the log-law region, which is a region where flow velocities can be estimated based on experimental research. This is shown in figure 2.2. However, the use of wall functions is limited when flow separation occurs (Stankovic et al., 2014). In that case it is better to resolve the viscous sublayer, for which the y^+ of the first grid cell should be around 1. By decreasing the y^+ value of the first grid cell, the amount of grid cells in the whole model domain will increase and hence the computation time. Therefore this last method is only advised for regions that have a large impact on the flow (ANSYS Inc., 2014).

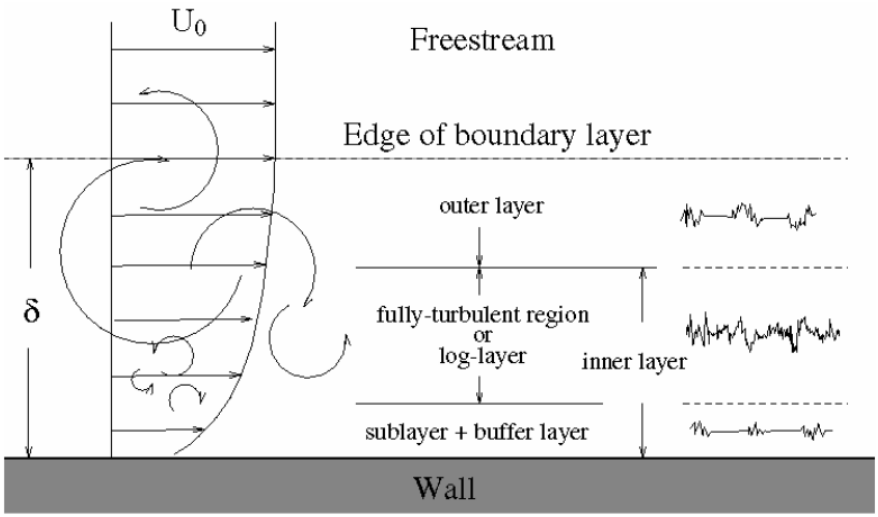

Figure 2.1: Various parts of the boundary layer present near a wall (ANSYS Inc., 2014)

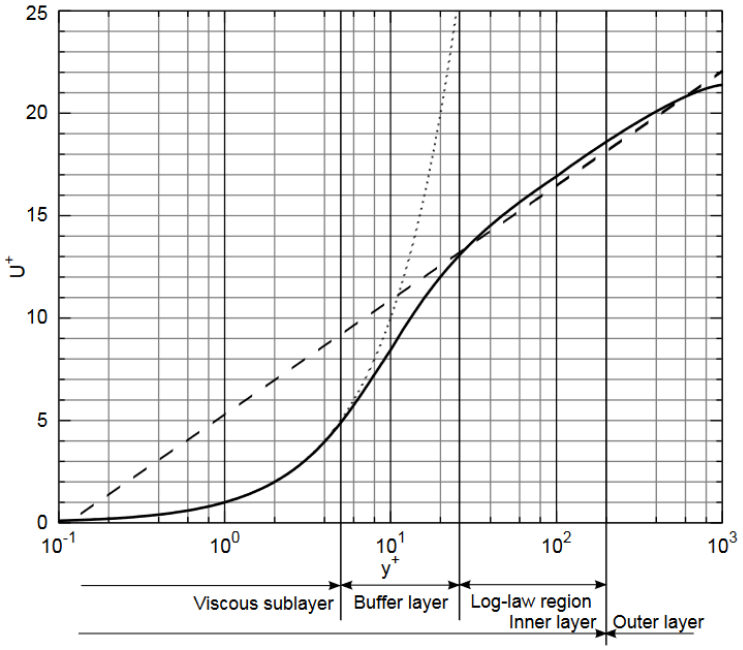

Figure 2.2: Behavior of velocity profile close to a wall, where the solid line is based on experimental data and the dotted and striped line are empirically derived equations (ten Pas, 2016).

2.4 Numerical equations and residuals

In order to simulate the transport of flow through the model domain, numerical models use spatial discretization schemes to calculate the values of various properties at the internal faces between grid cells and reach model convergence. For the gradient scheme, there are three common methods: Green-Gauss Cell Based, Green-Gauss Node-Based and Least-Squares Cell-Based. A Node-Based method is more accurate than a Cell-Based method, however this method is computationally very expensive. Results from the Least-Squares method are comparable to the results of the Node-Based method on irregular meshes, and less computationally expensive (ANSYS Inc., 2009a).

For the resulting flow properties such as the momentum or TKE, there are two popular schemes: First-Order Upwind and Second-Order Upwind. A second-order method is preferred over a first-order method, as the results are more accurate. A first-order scheme can lead to faster convergence, which is why it is sometimes used to start a run, before switching to second-order (ANSYS Inc., 2009b).

In order to check the convergence of a numerical model, residuals play a role. Residuals are the difference between numerical iterations for aspects such as the flow velocity in the x-direction or the momentum equation. The lower the residuals, the more accurate the solution will be. Once the residuals criterion is reached, the solution will have converged. If the solution does not seem reasonable after convergence, it is necessary to lower the residuals criterion or to improve the model setup (ANSYS Inc., 2010).

3 Method

The research is carried out in several steps. The first step is the construction of a numerical model with a single vegetation patch using a RANS turbulence model. Various model settings are evaluated and the model with the selected setup will be validated with experimental data, which provides an answer to research question 1. The second step consists of adding a second vegetation patch and varying its location and density, which will give an answer to research question 2. The last step involves the choice of a threshold velocity and threshold turbulent kinetic energy for sediment deposition, based on other research, and the evaluation of the possible deposition patterns. This will provide an answer to research question 3. All previously mentioned steps are shown in figure 3.1 and discussed in more detail in the next sections.

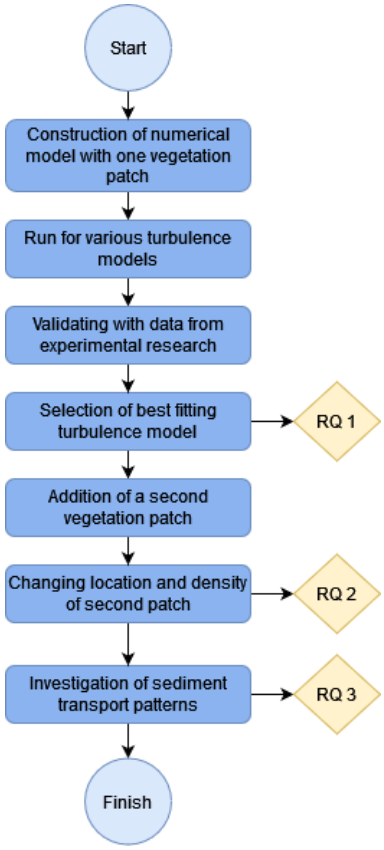

Figure 3.1: Flowchart of the steps to perform in order to achieve the research objective

3.1 Isolated patch

In order to analyse the flow velocities and turbulence levels around two patches of different densities, it is first of importance to set up a reliable model. This is done by constructing a model with a single vegetation patch and comparing it to experimental data. The experimental data used for the validation is the research by Zong and Nepf (2012). They performed multiple flume experiments with simplified, emergent vegetation patches, which were represented by several cylinders placed in a circular manner.

3.1.1 Model choice and setup

The model chosen for this research is Ansys Student 2022 R1 with the solver Fluent, hereafter referred to as FLUENT®. The choice for this model was based on the research by de Lima et al.

(2015), as they have successfully used the same program for similar research. The largest limitation with the Ansys Student R1 version is with the maximum amount of cells that the program allows. This is limited to 512,000 cells, which means that there is a restriction on the size of the model domain or the resolution of the grid.

As the reference model is validated with the data of Zong and Nepf (2012), their dimensions will dictate the model setup. Zong and Nepf (2012) had access to a flume of 13 meters long and 1.2 meters wide. As this research will be executed in the 2D plane, the depth of the flume is not of importance. de Lima et al. (2015) concluded that with emergent vegetation the most prominent flow patterns will happen in the horizontal plane and therefore neglect the influence of the smooth bed. As this study is interested in the flow velocities and the turbulence generated by an emergent vegetation patch, similar to de Lima et al. (2015), the focus will be on the flow in the middle of the vertical section. The vegetation patch selected for model validation has a diameter of 22 cm and a solid volume fraction of 3%. Figure 3.2 shows the velocity profile measured by Zong and Nepf (2012) behind a single patch with these characteristics. These measurements were taken with a probe, which was setup with a positioning accuracy of ± 1 cm in the x-direction and ± 0.5 cm in the y-direction on the centerline behind the patch. No measurements were taken inside the patch, due to difficulties with placing the probe inside the patch. The undisturbed upstream velocity was 0.098 m/s with an uncertainty of ± 0.05 m/s (Zong and Nepf, 2012). In Figure 3.2 it is visible that the flow velocities behind the patch are much lower than in front of the patch, as this is steady wake region. At a certain distance behind the patch, the centerline velocity starts to increase, which is the point at which mixing occurs and the steady wake region ends, as also explained in Section 1.1. The length of the steady wake was determined to be $8D$, with an uncertainty of ± $0.5D$ (Zong and Nepf, 2012).

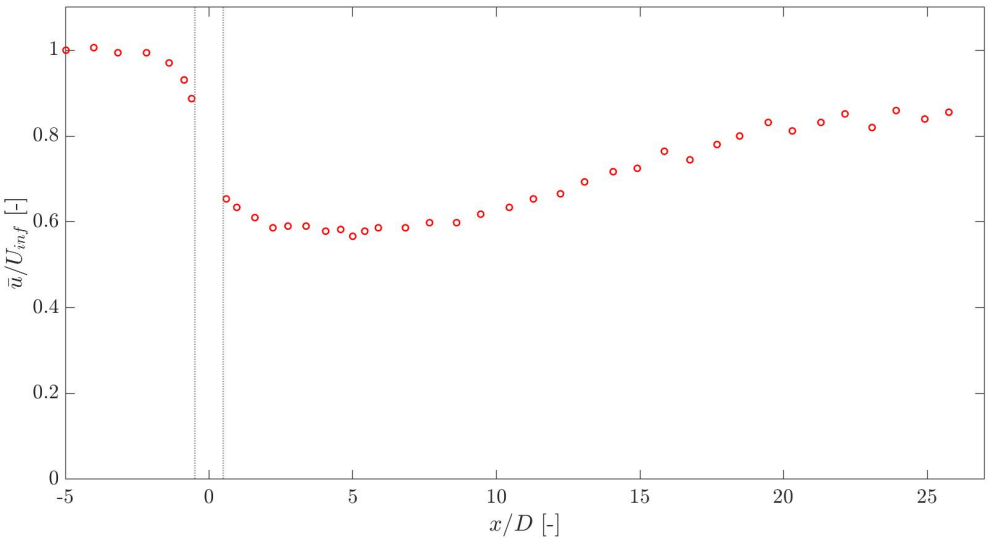

Figure 3.2: Normalized velocities on the centerline behind a single vegetation patch of ϕ=3%, measured by Zong and Nepf (2012).

In the setup by Zong and Nepf (2012), the edge of the patch was located 3 meters from the flume inlet. Due to the limitation on the amount of grid cells and to keep the computational time low, the choice was made to zoom in on the areas of interest and only have those areas represented in the model. Areas of interest are found directly upstream and downstream of an obstacle, and on both sides of the obstacle. These are regions where flow diversion occurs and turbulence spikes due to the presence of an obstacle. From several test runs it was found that the flow diversion in front of the obstacle did not occur more than 4.5D in front of the obstacle, which is why this distance

was selected for the domain. At the other side of the flume, at the outlet, some length was also removed in such a way that the area behind the patch has a maximum length of 40D. As areas of interest are also present at the sides of an obstacle, the width of the domain is the same as by Zong and Nepf (2012), which is 1.2 meters. A schematized setup of the model is shown in Figure 3.3.

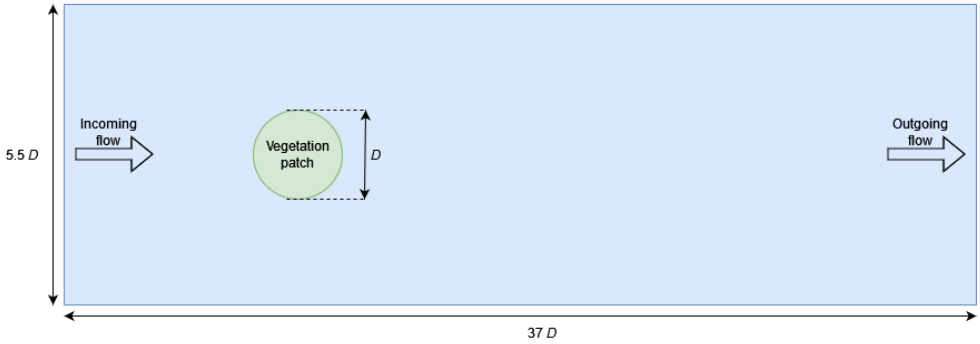

Figure 3.3: Schematization of the model domain for a single vegetation patch

Due to the limit of 512,000 cells, it is important to carefully distribute the areas with finer and coarser grid. For this research, the flow properties in the middle of the domain are of interest, which means that the physics at the sidewalls are not relevant. For these regions, wall functions will be used and the grid cells will be placed in such a way that the appropriate y^+ value (y^+>30) is achieved. On the other hand, the boundary layers around stems of the vegetation patches are areas of interest. Since flow separation occurs in these areas, wall functions are not recommended and therefore the viscous sublayer will be resolved by creating a very fine mesh around the stems. Preferably, the y^+ of the cells around the cylinders is around 1, but when this is unachievable due to grid cell limitations, a maximum value of 5 is acceptable to ensure that the first cell is still in the viscous sublayer, as seen in Figure 2.2. Grid cells within the areas of interest, such as in the wake or in front of the vegetation patches, will also be refined to get a more accurate view of the physics in those regions. The distribution of finer and coarser grid cells can be seen in Figure 3.4a, which show a structured mesh in which rectangular grid cells are used.

A vegetation patch can be constructed by placing the individual stems in a circular shape, as Zong and Nepf (2012) did in their flume experiments. Circular patches with either 19 or 37 stems are studied. A square patch is also considered because this was used by de Lima et al. (2015) in their computational model and showed good agreement for the same validation data. Furthermore, Vandenbruwaene et al. (2011) observed similar flow patterns for a square and a circular shaped patch, which makes an interesting investigation to see if the same applies to this research as well. Square patches with either 16 or 36 stems are considered. To obtain the desired solid volume fraction with the limited availability of stems, the dimensions as shown in table 3.1 are used. The shape of a circular patch is shown in Figure 3.4b and the shape of a square patch is shown in Figure 3.4c.

The fine grid around the stems is achieved by placing a square around each stem. With a bias function the cells next to the stem are much smaller. This can be seen in Figure 3.4d. Varying the amount of cells and changing the bias will influence the y^+ value.

Table 3.1: Four different patch shapes and corresponding characteristics

Shape	**Nr of stems**	**Patch diameter [cm]**	**Stem diameter [cm]**
Circle	37	22	0.6264
Circle	19	22	0.8742
Square	36	22	0.7166
Square	16	22	1.0749

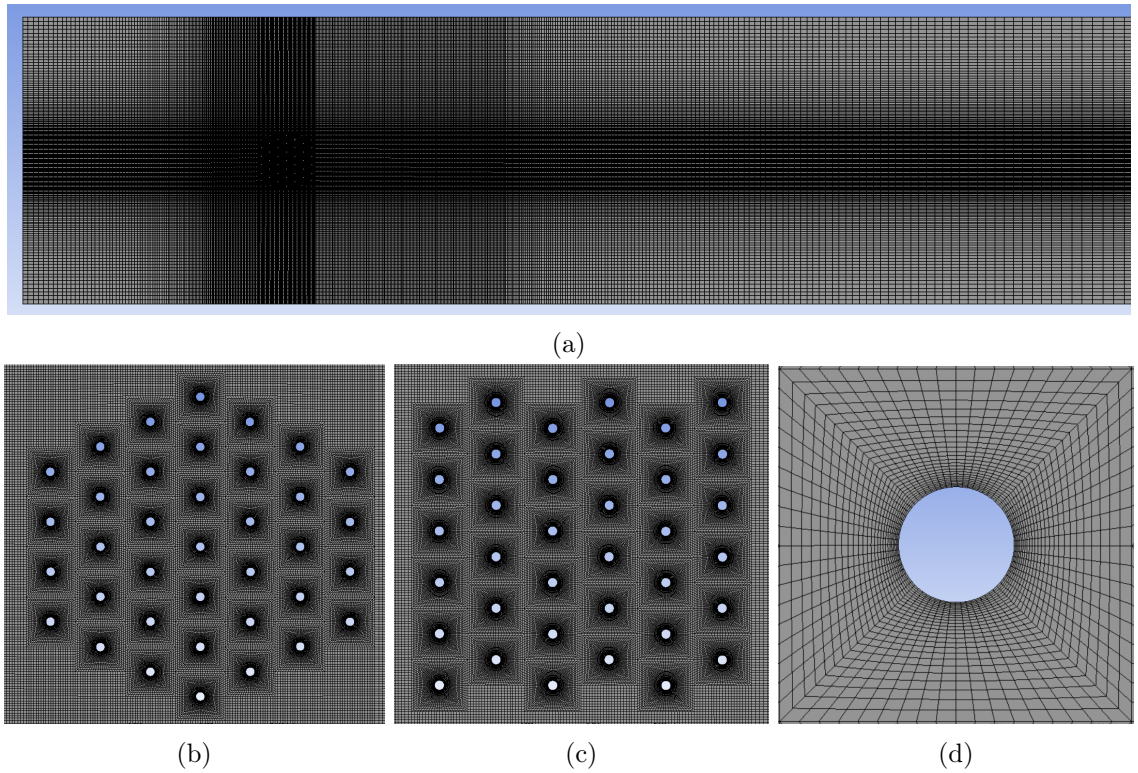

(a)

(b) (c) (d)

Figure 3.4: Gradual zoom in on the model domain with one patch, showing a large part of the model domain, in which the darker areas signify a finer mesh and the lighter areas a coarser mesh (a), a close-up of a circular vegetation patch with 37 stems (b), a square vegetation patch with 36 stems (c), and the distribution of cells around a single vegetation stem (d).

3.1.2 Boundary conditions

The inlet is defined as a velocity inlet, where the velocity is set to a constant speed of 0.098 m/s. This is in line with the experiments performed by Zong and Nepf (2012), which also have a constant upstream velocity of 0.098 ± 0.005 m/s. The outlet is a pressure outlet, which is set to a constant 0 Pa. The walls of the domain and the walls of the stem cylinders are smooth and defined as no-slip, which means that the velocity of the fluid layer that is in contact with the boundary is 0 m/s (Rapp, 2017). Further model specifications are given in Appendix A.

3.1.3 Model settings and validation

First an analysis is performed to investigate how reactive the model is to the input boundaries. Zong and Nepf (2012) state in their research that the upstream velocity was 0.098 m/s with an uncertainty of ± 0.05 m/s. Therefore the reference case is also tested for an upstream velocity of 0.103 m/s and 0.093 m/s. Another factor of interest is the turbulence intensity. Turbulence intensity (TI) describes the amount of turbulence as a percentage. When there are little to no fluctuations in a flow, the TI is between 0 and 1%. A highly turbulent flow usually has a TI of 10% or more. The standard value for TI in FLUENT® is set at 5% (ANSYS Inc., 2009b). Experimental measurements performed by Mcquivey (1973) show that in a flume of 1.22 meters wide, which is about the same width as this research, the TI in the middle of the horizontal and vertical section is around 3 to 4%. This flume also has a smooth bed, which is similar to the experiments of Zong and Nepf (2012). This leads to the decision to test the model for a TI of 2, 4, 5 and 10%. All these different scenarios, which are tested and compared against each other, are given in Table 3.2. These different runs are all performed with a circular patch, consisting of 37 stems. The selected

turbulence closure model is the standard $k-\epsilon$ model with Menter-Lechner wall functions.

Table 3.2: Different upstream velocities and turbulence intensities that are compared against each other

Scenario	**U_{inf} [m/s]**	**TI**
1	0.098	5%
2	0.093	5%
3	0.103	5%
4	0.098	2%
5	0.098	4%
6	0.098	10%

After the initial conditions have been evaluated and the best fitting ones are selected, the different patch shapes mentioned in Section 3.1.1 and Table 3.1 will be tested. Step 1 in Table 3.3 shows the scenarios with the different patch shapes that will be compared against each other. Initial runs showed that different patch shapes give varying results depending on the selected turbulence closure model. Therefore the two best performing patch shapes will also be tried for the following turbulence closure models: $k-\epsilon$, realizable $k-\epsilon$, RNG $k-\epsilon$ and $k-\omega$ SST. In step 2, the additional runs are done with the best performing patch shape determined with scenarios from step 1. As the $k-\omega$ SST model did not converge, this run is no longer included. For scenarios 1, 3, 5, 6, 7 and 8, the steady wake length behind the patch will be compared to the data of Zong and Nepf (2012), as well as the centerline velocity in the longitudinal direction and the velocity across the flume width at $x = 4.5D$.

Table 3.3: Different patch shapes and turbulence closure models that are compared against each other

Step	**Scenario**	**Turbulence closure model**	**Wall function**	**Patch shape**	**Nr of stems**
1	1	Standard k-epsilon	Menter-Lechner	Circle	37
	2	Standard k-epsilon	Menter-Lechner	Circle	19
	3	Standard k-epsilon	Menter-Lechner	Square	36
	4	Standard k-epsilon	Menter-Lechner	Square	16
2	5	Realizable k-epsilon	Standard	Circle	37
	6	Realizable k-epsilon	Standard	Square	36
	7	RNG k-epsilon	Standard	Circle	37
	8	RNG k-epsilon	Standard	Square	36

The model with the patch shape that shows the best agreement with the validation data will be evaluated further by alternating between different wall functions. As different wall functions in combination with different turbulence closure models have an effect on the simulated velocities, this is an important test to get a complete idea of how well the model is able to represent the validation case. The turbulence closure model and wall function that shows the best agreement in terms of steady wake length, centerline velocity profile in the longitudinal direction and transverse velocity profile in the longitudinal direction at 4.5D behind the patch is then selected as input for research question 2, as explained in the next section. Scenarios for the different turbulence closure model and wall function combinations are presented in Table 3.4.

Table 3.4: Different turbulence closure models and wall functions that are compared against each other

Scenario	Turbulence closure model	Wall function
1	Standard k-epsilon	Standard
2	Standard k-epsilon	Scalable
3	Standard k-epsilon	EWT
4	Standard k-epsilon	Non Equilibrium
5	Standard k-epsilon	Menter-Lechner
6	Realizable k-epsilon	Standard
7	Realizable k-epsilon	Scalable
8	Realizable k-epsilon	EWT
9	Realizable k-epsilon	Non Equilibrium
10	RNG k-epsilon	Standard
11	RNG k-epsilon	Scalable
12	RNG k-epsilon	EWT
13	RNG k-epsilon	Non Equilibrium

3.2 Two vegetation patches with different densities

After defining the model settings and validation of the reference model with experimental data from Zong and Nepf (2011), a second vegetation patch will be added. A schematization of the new model is shown in Figure 3.5. The two patches will each have a different density, which is defined by the solid volume fraction. In doing so, the effect of these different densities on the steady wake length behind the upstream or downstream patch, and the effect on the flow velocities and turbulent kinetic energy in the entire flow domain can be evaluated. The model domain has the same width as in the reference case, however the length downstream of the patches is increased by $5D$ to account for the presence of the downstream patch. Rominger and Nepf (2011) and Meire et al. (2014) both found in their experimental studies that the upstream adjustment length is dependent on the diameter of the patch, not on the density. Therefore the choice for an upstream distance of $4.5D$ is also valid for patches with higher densities. The choice is made to remove the function of the outer walls that are on both sides of the cylinder and replace them by so-called 'symmetry planes'. "Symmetry boundary conditions are used when the physical geometry of interest, and the expected pattern of the flow/thermal solution, have mirror symmetry." (ANSYS Inc., 2009b) Using symmetry planes means that the effect of a wall is taken away, and the flow diverting around both cylinders is not affected by potential drag caused by these walls. The motivation for this choice is that the sidewalls would have a larger effect on the patches as they are moved closer to the sidewalls. An additional benefit is that, by doing this, the results of the effects of different densities can be applied to many situations and are not just representative for a flume or river of exactly 1.2 meters wide.

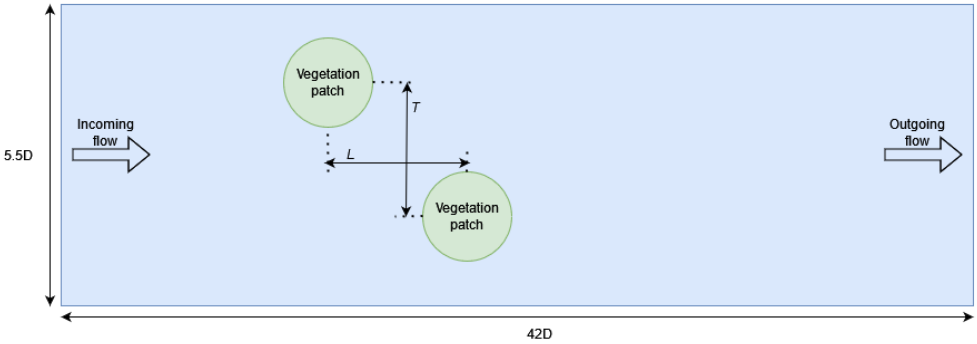

Figure 3.5: Schematization of the model domain with two vegetation patches

The different upstream and downstream patch densities and transverse and longitudinal distances that will be considered are presented in table 3.5. All patches have the same diameter and the density is altered by changing the diameter of the stems. The densities that are evaluated are based on densities used in previous research. Section 1.2 mentions that both de Lima et al. (2015) and Yamasaki et al. (2019) use patches with a solid volume fraction of 10%. Kitsikoudis et al. (2020) used patches with a solid volume fraction of 6%, 11% and 19% and classified them in that order as sparse, medium and dense. Meire et al. (2014) selected patches with a solid volume fraction between 3.3% and 11%, and Zong and Nepf (2012) use patches with a solid volume fraction between 3% and 36%. In this research, a vegetation patch with a solid volume fraction of around 10% is considered to be of medium density. The decision was made to evaluate a range of densities between ϕ=0.03 and ϕ=0.19, where the patch of interest would always have a density of ϕ=0.10.

The longitudinal and transverse distances that are compared are based on research by de Lima et al. (2015) and Kitsikoudis et al. (2020). de Lima et al. (2015) found that there is always enhanced sediment deposition for T<1.3D and no patch interaction for L>6D. Kitsikoudis et al. (2020) placed their staggered patches at L=3.5D and T=1.5D. From this experimental research, the most noteworthy results were found by keeping the upstream patch the same density and changing the density of the downstream patch. Therefore three different scenarios are tested for the a change in density of the downstream patch: T=1.3D and L=4D, T=2.5D and L=4D, and T=1.3D and L=6D. For a change in density in the upstream patch only one scenario is tested: T=1.3D and L=4D. All different runs and corresponding densities are shown in table 3.5. The distances T/D and L/D refer to the interpatch distances, as shown in Figure 1.2b. After completion of the planned runs, the results will be compared to each other, in which the centerline velocity and centerline TKE behind the medium patch will be of special interest.

Table 3.5: Planned runs and patch densities for the different interpatch distances

Run	Density upstream [-]	Density downstream [-]	T/D [-]	L/D [-]
1	0.10	0.03	1.3	4
2	0.10	0.06	1.3	4
3	0.10	0.09	1.3	4
4	0.10	0.12	1.3	4
5	0.10	0.14	1.3	4
6	0.10	0.19	1.3	4
7	0.10	0.06	2.5	4
8	0.10	0.14	2.5	4
9	0.10	0.19	2.5	4
10	0.10	0.06	1.3	6
11	0.10	0.14	1.3	6
12	0.03	0.10	1.3	4
13	0.06	0.10	1.3	4
14	0.19	0.10	1.3	4

3.3 Enhanced sediment deposition and vegetation growth

The evaluation of the sediment deposition is based on the research by Ortiz et al. (2013). They found that not only does the flow velocity have an effect on the sediment deposition, but that the turbulent kinetic energy also plays a role. In a flume without vegetation patches they found that there is a certain amount of sediment that is deposited evenly throughout the flume, called the control volume. The addition of a vegetation patch disturbs this control volume by creating patterns of enhanced sediment deposition, in which there is more sediment deposited than the control volume; or erosion, in which there is less sediment deposited than the control volume. As this study is performed with a 2D model that simulates flow in the middle of the water column, it is not realistic to study erosion processes as they are much related to flow properties close to the bed. For their classification of a sparse patch, Ortiz et al. (2013) found that enhanced sediment deposition only occurs if both the velocity and TKE are below the open channel values upstream of the patch. For a dense patch, 89% of the enhanced sediment deposition occurred in areas where these conditions were met, although it was also observed that some sediment was deposited for higher TKE values. The density of the patches used by Ortiz et al. (2013) is defined by aD, which is around 8.4 for the dense patch and 2.5 for the sparse patch. For comparison, the most dense patch used in this research gives $aD = 2.4$, which means that it would still be considered a sparse patch according to Ortiz et al. (2013). Because of this, when assigning areas of enhanced sediment deposition, the only regions that qualify are regions where both the flow velocity and TKE values are below the upstream open channel values. The upstream open channel value of velocity is equal to the velocity selected for the inlet boundary condition. The open channel value for the TKE is calculated with the turbulence intensity and based on an empirical correlation, as shown with Equation (12) (ANSYS Inc. 2009b; Langtry and Menter 2009).

$$k = \frac{3}{2}(U_{inf} I)^2 \tag{12}$$

Where:

- U_{inf}: undisturbed upstream velocity [m/s]
- I: Turbulence Intensity [-]

The results from the runs shown in Table 3.5 are used for this evaluation. The area of the grid cells in which, by this reasoning, enhanced sediment deposition could occur are compared to the total area of the study domain. This will result in a percentage of enhanced sediment deposition for each type of simulation. These located areas of enhanced sediment deposition could then give an indication of where new vegetation growth can take place.

A problem with the velocity and TKE method described in section 3.3 is that the initial value, and thus open channel value, is determined with an empirical equation that is based on experimental data, in which bed friction plays a role. As mentioned in section 4.2 and seen in Figure 4.9, with a 2D model, bed friction is no longer taken into account which leads to a drop in TKE compared to the initial value. As such, the TKE in front of the upstream patch will always be lower than the initial value. Therefore the choice was made to remove the information on sediment deposition in front of the patch, as this is not trustworthy. Behind the patch, the turbulence generated by the patch is dominant over the turbulence induced by the bed friction (Zong and Nepf, 2012). Therefore this method is valid for evaluating enhanced sediment deposition behind the patch.

The velocity and TKE method is compared to the method used by de Lima et al. (2015), where they use a threshold velocity of u/U_{inf}=0.7. This value is roughly based on a coarser type of sediment and the velocity that is necessary to keep the grains in motion. If the velocity is lower than this, sediment deposition takes place. This is then applied to the modelling domain of this study, where the area that meets this condition is compared to the total area. To see if there are similarities between both techniques, this new percentage will be compared to the percentage that is derived with the other method.

4 Results

4.1 Velocity profiles of the reference model

In this section, the results of the reference case are shown and discussed. The chosen RANS model uses the Navier-Stokes equations explained in Section 2, to calculate time-averaged velocities behind an individual patch. Simulations are performed with different inlet conditions, patch shapes and turbulence closure models, in order to find a combination that gives results that are closest to experimental observations. This combination will then also be used for the following research questions of this study.

4.1.1 Influence of initial conditions

A sensitivity analysis is performed to measure the influence of the initial conditions. Figure 4.1 shows the simulated centerline velocities in front of and behind the patch. The figure shows that changing the upstream velocity and the TI do not have large influence on the normalized flow velocities in the wake. The largest difference between two runs was found to be 1%, between the runs with a TI of 2% and 10%. However this difference is minimal and where the run with a TI of 10% is closer to the experimental measurements in the steady wake region, the opposite is the case during the flow recovery. Therefore the decision was made to keep the upstream velocity at 0.098 m/s and to keep the TI at 5%.

As seen from Figure 4.1, no validation data is available of the flow behaviour inside the vegetation patch. This lack of data in combination with the employment of a RANS model, which is not expected to provide accurate results on small-scale turbulence, led to the decision to dismiss the simulated velocity and TKE values in between the patch. This will also be done for all future velocity and TKE profile plots.

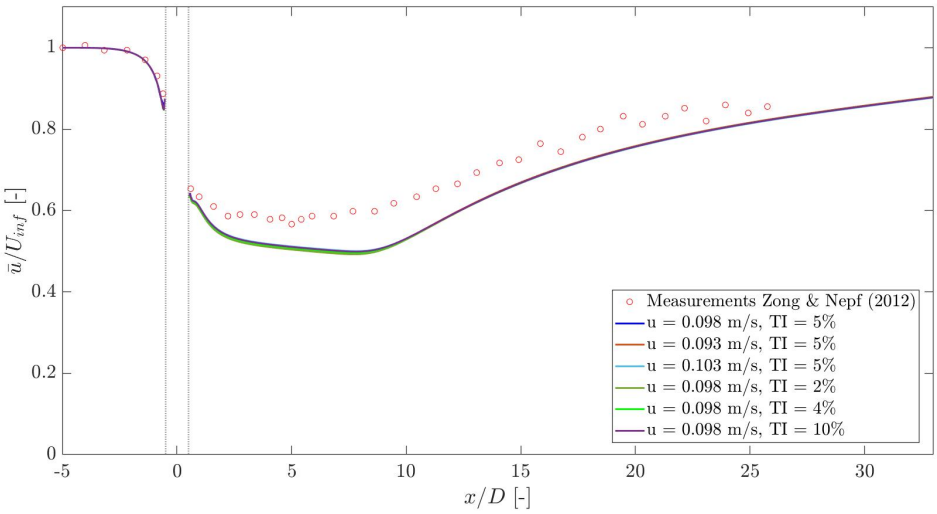

Figure 4.1: Normalized longitudinal velocities for a single vegetation patch for different upstream flow velocities or turbulence intensity.

4.1.2 Influence of the shape of the vegetation patch

The influence of a different patch shape is evaluated by how well the simulated data corresponds to the measured data of Zong and Nepf (2012). Two values are of importance: the simulated velocities and the steady wake length. The steady wake is the region behind the patch where the flow velocity is low. This region ends when the longitudinal flow velocity increases, meaning that the flow starts

to recover towards its upstream value. The steady wake length of the measured flow from Zong and Nepf (2012) is around $8D$. The agreement between the simulated and measured velocity is evaluated by the maximum difference between the datasets. Simulations with different patch shapes and stem numbers showed that the models with fewer stems (16 or 19) were not as representative for the validation data as the shapes with more stems (36 or 37), as seen in figure 4.2. For the patches with fewer stems, the simulated flow velocities are overestimated in the region of the steady wake (from x/D=0.5 to about x/D=13), and underestimated in the region where mixing occurs (x/D=13 and beyond). A plot of the transverse profile of the normalized longitudinal velocity at distance $y = 4D$ behind the centre of the patch is shown in Figure 4.3. Again the patches with fewer stems are unable to measure up to patches with more stems. A strange feature of this plot is that the simulated velocity profile is constant throughout most part of the flow domain, where more of a curved profile would be expected, as is given by the experimental data. A possible explanation could be that the model underestimates the drag caused by the outer wall at y=2.7D. This can either be caused by applying the wrong boundary conditions for the wall, due to limitations of the used wall function or insufficient grid resolution. When wall-related drag increases, the velocity difference between the boundary layer and the rest of the domain increases. Due to the conservation of mass and momentum, this means that flow velocities in the middle of the domain would increase, much like as is shown with the experimental data.

The resulting choice is either the square patch with 36 stems or the circular patch with 37 stems, where the square patch shows better agreement with the data set. Continuing to model with this shape patch would mean that the simulated velocities in the model domain are more reliable compared to the simulated velocities of the circular patch. On the other hand, the circular patch seems to follow the shape of the data better, and is therefore more reliable when analyzing the steady wake length behind a vegetation patch. Ideally one of these two remaining patch shapes would score well on both criteria: similar velocities and an equal wake length to the validation data, as both are of interest for the succeeding model runs. Both the square 36 patch and the circular 37 patch will therefore be evaluated further.

As mentioned in section 2.2, applying the realizable $k-\epsilon$ and RNG $k-\epsilon$ models might improve the results. A $k-\omega$ SST model is also tested, but this run did not converge, which consequently means that the generated results cannot be trusted. Figure 4.4 shows centerline velocities for the runs with these different turbulence closure models for both the circle with 37 stems and the square with 36 stems. As both models do not reach convergence with the Menter-Lechner wall function, a standard wall function has been selected. A circular patch with the RNG $k-\epsilon$ model shows the best agreement with the measured data. The steady wake length for the circular patch is $9.2D$ and the maximum difference between the measured velocity and simulated velocity is 11%. Another option that comes close to the circular patch is the square patch with the RNG $k-\epsilon$ turbulence closure model. The maximum difference for this model is 12%, however the steady wake length extends up to $11.4D$ behind the patch. Therefore the circular patch with 37 stems is selected for the continuation of this research.

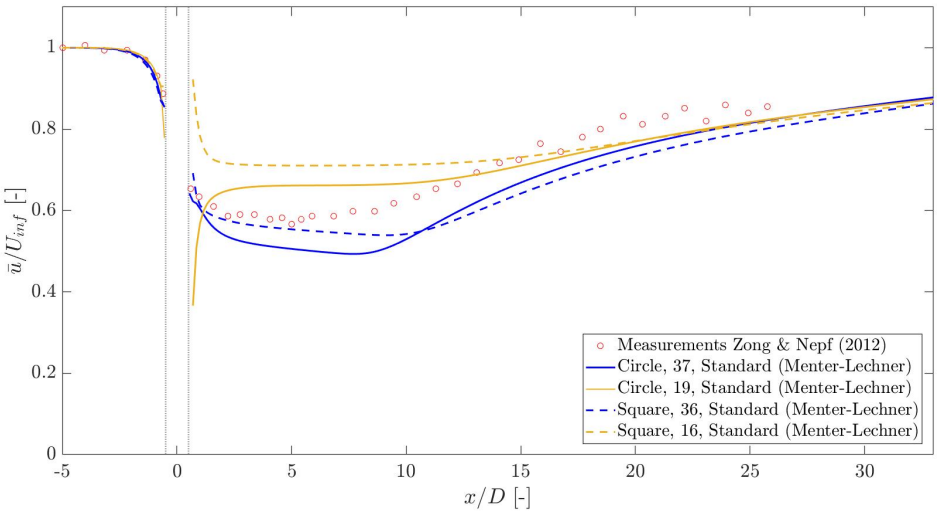

Figure 4.2: Normalized longitudinal velocities for a single vegetation patch with either a square or circular shape. The number behind the shape indicates the amount of stems within the vegetation patch.

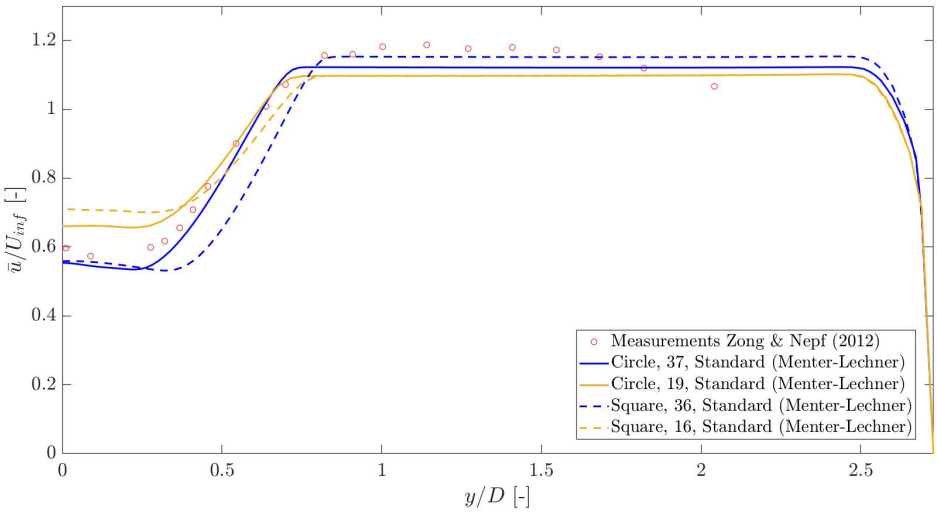

Figure 4.3: Transverse profile of the normalized longitudinal velocities for a single vegetation patch with either a square or circular shape at $4D$ downstream of the centre of the patch. The number behind the shape indicates the amount of stems within the vegetation patch.

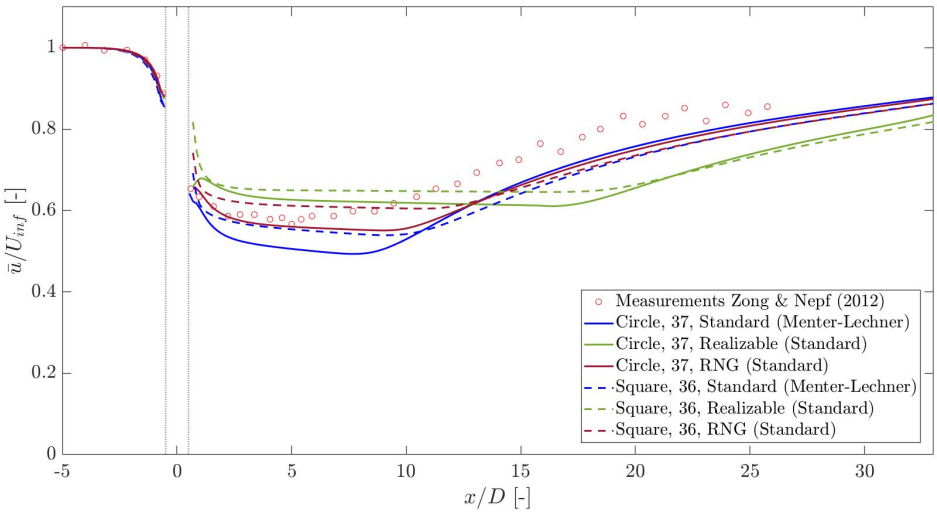

Figure 4.4: Normalized longitudinal velocities for a single vegetation patch with either a square or circular shape. The number behind the shape indicates the amount of stems within the vegetation patch. The turbulence closure model is indicated with the selected wall function between in parenthesis.

4.1.3 Influence of different turbulence closure models and wall functions

As a last validation step, the selected model shape will be tested for different combinations of turbulence closure models and wall functions, which have been discussed in more detail in Section 2. It proved difficult to reach model convergence with the application of the $k-\omega$ SST turbulence closure model. Therefore it was decided to continue the research only with the $k-\epsilon$ model, the realizable $k-\epsilon$ model and the RNG $k-\epsilon$ model.

Figure 4.5 shows the results of different turbulence closure models and wall functions that were applied to a single circular patch with 37 stems. It is worth noting that the realizable $k-\epsilon$ model consistently overestimates the length of the steady wake region, whereas the standard $k-\epsilon$ model tends to underestimate the flow velocity in the steady wake length. The RNG $k-\epsilon$ turbulence closure model with standard wall functions is still the best fit, with a maximum difference of 11% and a steady wake length of $9.2D$ compared to the measured steady wake length of $8D$ from Zong and Nepf (2012). It is remarkable that these different turbulence closure models and wall functions give such different results for the same model setup. This is caused by the difference in equations from which each type of model and wall function is made up (ANSYS Inc. 2014; ANSYS Inc. 2009b). Generally, the best agreement would have been expected with EWT (Enhanced Wall Treatment), as this is a y^+ insensitive method, and will therefore definitely not give problems due to the y^+ value around the stems being less than 5 (ANSYS Inc., 2014). That this is not the case only proves that validation with experimental data is very important and that there is no universally correct or best turbulence closure model to apply to all scenarios.

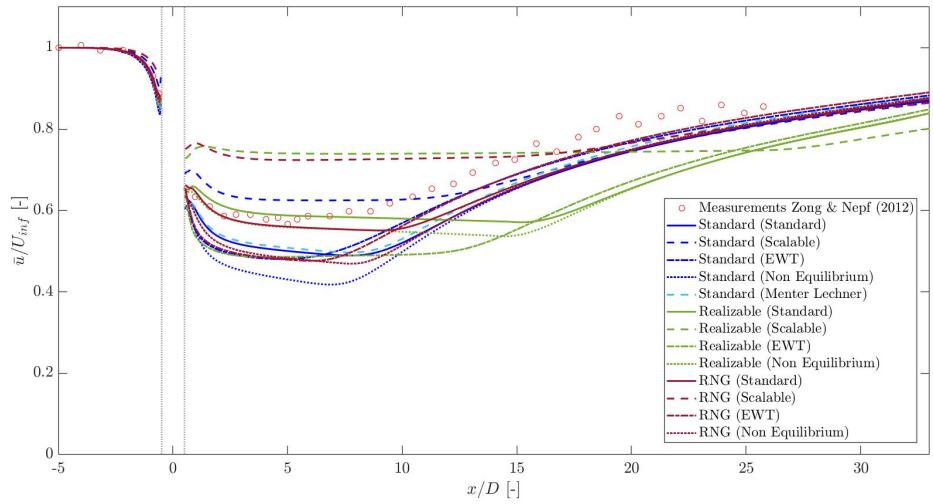

Figure 4.5: Normalized longitudinal velocities for a single vegetation patch for different variants of the $k-\epsilon$ turbulence closure model and various wall functions.

4.2 Two patches in staggered arrangement

After the completion of the model validation, a circular patch with 37 stems proved to generate the most realistic results. Due to the limitation on the number of cells, it is not possible for both patches in a staggered setup to have 37 stems. Therefore the choice is made to introduce one patch with only 19 stems and compensate for the density by increasing the stem diameter. This choice will inevitably result in additional uncertainty of the model output. Only the wake behind the patch of 37 stems is analyzed, which, depending on the type of simulation, is either behind the upstream or the downstream patch.

4.2.1 Influence on upstream patch

In the first four runs that are performed, the distance between the two patches is L=4D and T=1.3D, for different densities (ϕ=3, 6, 14 and 19%) of the downstream patch. Figure 4.6 shows the distribution of longitudinal velocities for one of the runs, in which the black lines show the lines along which the velocity and TKE profiles are taken. These velocity profiles and TKE profiles are shown in Figures 4.7 - 4.9.

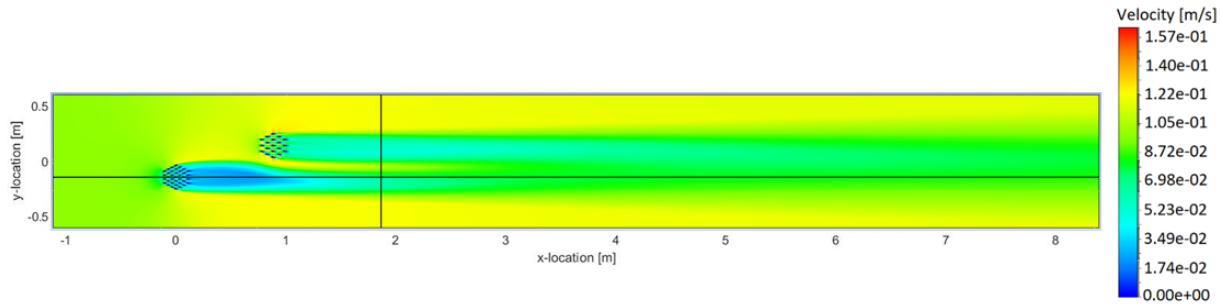

Figure 4.6: Distribution of longitudinal velocities throughout the model domain for an upstream patch of ϕ=10% and a downstream patch of ϕ=6%. The horizontal black line shows the location at which the velocity and TKE profiles are extracted. The vertical black line shows the location where the transverse velocity plots are extracted. The distance between the patch centers is L=4D and T=1.3D.

When the two patches are placed at a distance of L=4D and T=1.3D from each other, the steady wake of the upstream patch is affected by the presence of a downstream patch. This becomes clear in the longitudinal and transverse velocity profiles shown in Figures 4.6 and 4.7. In comparison to the single patch of equal density that is shown, the steady wakes behind the upstream patches are significantly shortened by the presence of a downstream patch. Interesting to see in Figure 4.7 is how much effect the density of a downstream patch has on the flow velocity. A denser downstream patch results in a shorter steady wake length behind the upstream patch, and generally contributes to generating higher flow velocities along the centerline. These effects make sense, as the flow around a dense patch experiences a larger flow diversion (Meire et al., 2014). Less flow can go through the patch, so a larger part of the flow has to go around it. This results in enhanced velocities on the sides of the downstream patch, which interfere with the wake of the upstream patch. For a denser downstream patch, the wake behind the upstream patch has a peak directly downstream of the location of the downstream patch. This is caused by the previously mentioned enhanced flow velocities mixing with the wake of the upstream patch. This is in line with the findings by Kitsikoudis et al. (2020). The dense patch that they used (ϕ=19%) showed a similar peak directly downstream of the location of the downstream patch, although the peak velocity measured by Kitsikoudis et al. (2020) stays below the value of the undisturbed upstream velocity, whereas the simulated velocities in Figure 4.7 go even higher. It is, however, not extremely trustworthy to compare exact numbers as the model validation in 4.1 showed that the generated velocity may deviate from the measured velocities. Furthermore, Kitsikoudis et al. (2020) used an upstream patch with a different density and different interpatch distances (L=3.5D, T=1.5D). For the sparse downstream patch (ϕ=6%) of Kitsikoudis et al. (2020) there is no such peak present in the wake of the upstream patch. This peak is also not present in Figure 4.7 for the two sparsest patches (ϕ=3 and 6%), meaning that these findings are in line with each other.

The fact that the steady wake length is longer for sparser downstream patches (Figure 4.7) means that mixing of the two wakes occurs further downstream in the domain compared to the denser patches. This is similar to the findings by Meire et al. (2014), who looked at two patches side-by-side, but also found that the merger of wakes occurred further downstream for sparser patches. This is explained by the level of turbulence generated by patches of different densities. For a denser downstream patch, the generated turbulence is higher and will therefore speed up the wake merger process.

The transverse profiles of the longitudinal velocities at $x = 8.5D$ are shown in Figure 4.8, for all downstream patches of different densities. These profiles clearly show the steep velocity gradients between the jet stream in between the two patches and the patch wake on each side. As sparser patches have a larger part of the flow going through the patch compared to denser patches, the amount of flow diverting around a sparser patch is smaller and has a lower flow velocity. This explains why the jet stream of the run with the sparsest downstream patch (ϕ=3%) is still located in between the two patches, which is between $y = 0.15D$ and $y = -0.15D$ (Figure 4.8). For denser downstream patches that create more flow diversion, the jet stream is pushed further out towards the wake of the upstream patch where mixing occurs. For denser downstream patches, this results in the velocity peak that is seen in Figure 4.7. The skewed profile in the wake of the sparser downstream patches can be attributed to the sparseness of the patch and the small amount of stems within that patch. The downstream patch has only 19 stems that are very small for a sparse case, which leaves room for very distinct streams of higher and lower velocities to exit the patch. Higher velocities in between the location of stems, and lower velocities behind stems. Due to the lower turbulence generated by the patch, these streams do not mix as fast as they would for a denser case. The jet stream in between the patches, shown by the velocity peak in the center of Figure 4.8, has a lower velocity than the flow velocity on the other side of the downstream patch. This difference is most significant for the two sparsest downstream patches, the patches with a density of ϕ=3% and 6%. One side of the wake of the downstream patch mixes with the lower flow velocities

of the jet stream, whereas the other side of the wake mixes with the enhanced velocity on the other side. This results in the displacement of minimum wake velocity towards the middle of the patches (Figure 4.8, $x/D = 0.15 - 1.15$). The uneven wake profile for the sparsest downstream patches is then a combination of the wakes behind the individual streams that have not yet mixed and the fact that the minimum wake velocity moves closer to the centerline.

Looking at the TKE profile presented in Figure 4.9, it is clear that a denser downstream patch results in a higher TKE peak in the wake of the upstream patch. This peak is located more upstream for a denser downstream patch compared to a sparser downstream patch. Due to the presence of the downstream patch, the two shear layers that are formed on either side of the upstream patch are forced to meet in the centerline further upstream than they would without the presence of a downstream patch. This occurrence indicates the end of the steady wake region and is the location where mixing takes place and turbulence levels rise. Depending on the density of the downstream patch, the flow diverting around that patch is either of a higher or lower velocity, as mentioned above. With higher velocities, there is a more intense mixing at the end of the steady wake region, which, for denser downstream patches, results in the high turbulence peaks that can be seen in Figure 4.9. With a denser downstream patch, the amount of flow that diverts around the downstream patch is also greater and therefore interferes earlier with the upstream patch wake compared to sparser patches. This explains why the TKE peak of the two densest patches is located around x=5D and the peak of the two sparser patches is around x=8D. The odd shape of the TKE profile in the wake of the upstream patch in combination with a downstream patch of ϕ=19% is explained by the amount of flow diversion around the downstream patch. The flow diverting around the downstream patch pushes the wake and shear layers of the upstream patch to the side. This phenomenon is made visible in the transverse profile in Figure 4.8, where the upstream wake profile next to a denser patch is pushed further away from the centerline than for a sparser patch.

These findings are not in line with the findings by Kitsikoudis et al. (2020). Although they did find that the TKE peak for a denser downstream patch was still higher than for a sparser downstream patch, the location of this peak was placed further downstream instead of upstream compared to a sparser neighbouring patch. A reason for this is not given, however these differences can be attributed to difference in modelling circumstances, as Kitsikoudis et al. (2020) have performed an experimental study, where uncertainties are introduced related to measurement techniques.

The normalized velocity profile of the individual patch (Figure 4.7) first shows a sharp decrease in velocity at the beginning of the steady wake, followed by a mild decrease in velocity throughout the rest of the steady wake. This is also observed by Chang and Constantinescu (2015), when analyzing single patches of similar density with an LES model.

In the plots for TKE, it can be seen that directly behind the inlet, the turbulence drops. Since the model is in 2D at mid-depth, bed friction does not play a role throughout the model domain, hence it does not generate additional turbulence. However the initial TKE, as calculated by the model and explained in section 3.3, is based on an empirical correlation for which bed friction was taken into account. This then results in the sudden drop when this factor falls away.

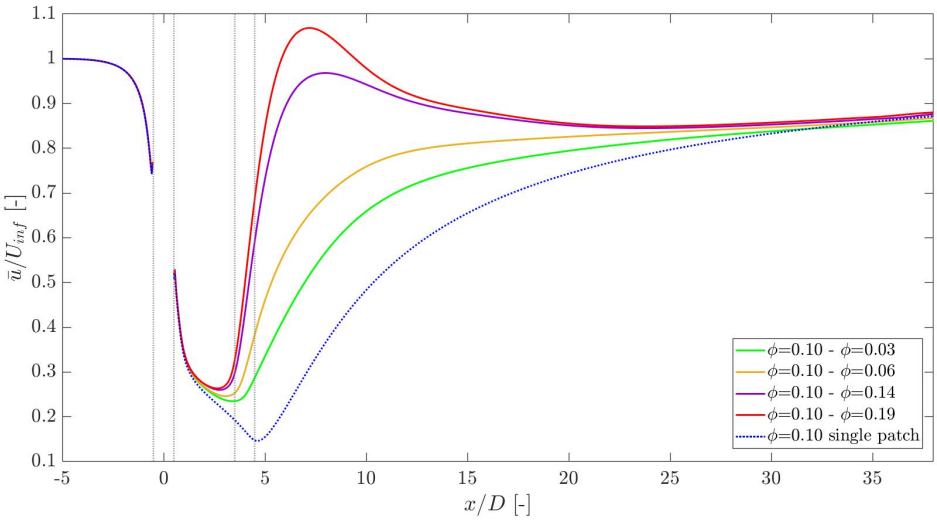

Figure 4.7: Normalized velocity profile through the centerline of the upstream patch as it is affected by a downstream vegetation patch with a different density. The grey lines show the location of the upstream patch and the downstream patch, with L=4D and T=1.3D. The legend shows the density ϕ of the upstream patch, followed by the density of the downstream patch.

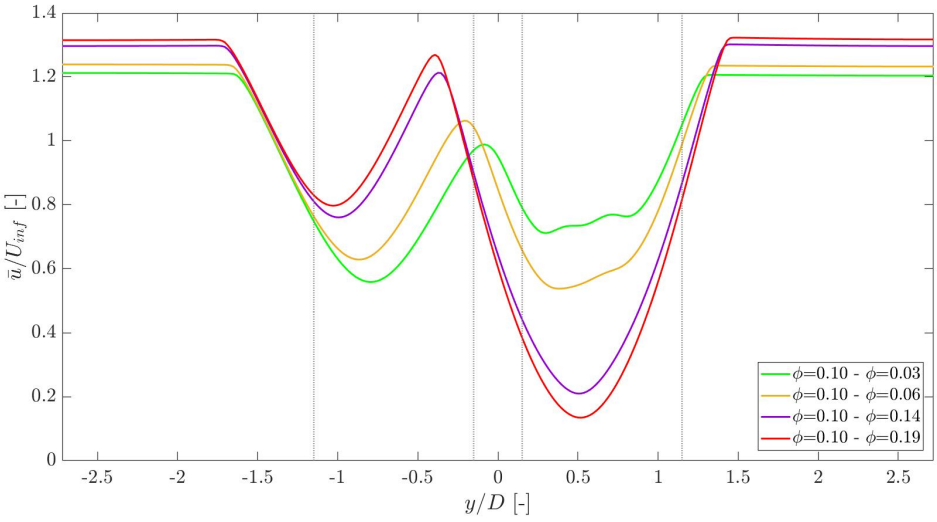

Figure 4.8: Transverse profile of the longitudinal flow velocities measured at a distance of 4.5D behind the downstream patch. The grey lines show where the patches are placed, the left lines represent the upstream patch and the right lines represent the downstream patch. The interpatch distances are L=4D and T=1.3D. The legend gives first the density ϕ of the upstream patch and then the density ϕ of the downstream patch.

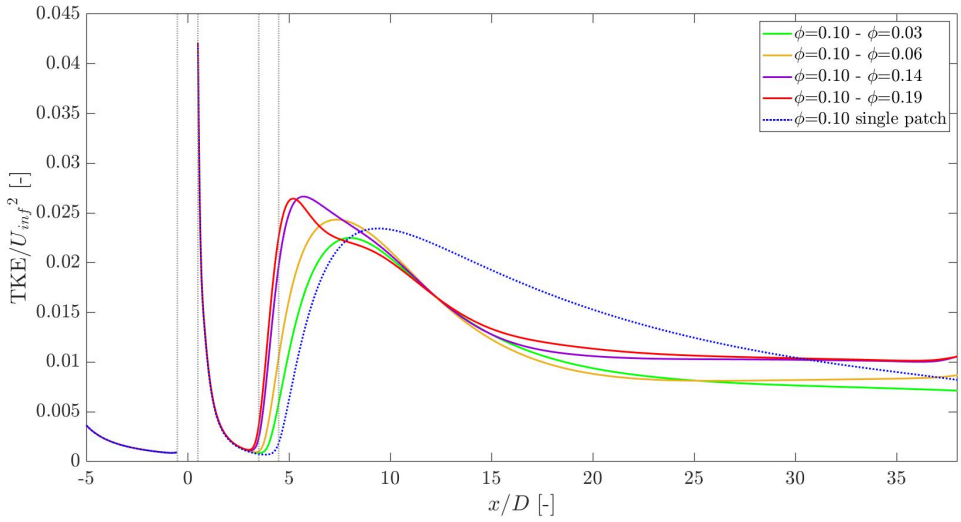

Figure 4.9: TKE profile through the centerline of the upstream patch as it is affected by a downstream vegetation patch with a different density. The grey lines show the location of the upstream patch and the downstream patch, with L=4D and T=1.3D. The legend shows the density ϕ of the upstream patch, followed by the density of the downstream patch.

For the next three runs, the two vegetation patches are placed further apart at L=4D and T=2.5D. The normalized longitudinal velocity profile of the upstream patch is shown in Figure 4.10. This profile is very similar to Figure 4.7, but much less pronounced. The velocity peak in the wake of the upstream patch that was first present at around $x = 7D$ for a downstream patch of density ϕ=14%, disappears when the patches are placed further apart in the transverse direction. What remains the same is that the wake velocity is higher for a denser downstream patch than for a sparser downstream patch. A remarkable effect with patches placed further apart, is that flow recovery takes place over a shorter distance than when the patches are closer together. As seen from Figure 4.7 and later in Figure 4.16, where the patches are placed with T=1.3D, but L=6D, the flow does not nearly reach the undisturbed upstream velocity at the end of the modelling domain. However, when the patches are placed further apart, the flow is already recovered between x=35D and x=37D. Figure 4.13 highlights these findings, as it shows the different velocity profiles for patches placed at different distances, where the downstream patch has the same density of ϕ=14%. This rapid recovery is the case for all downstream patch densities, although a sparser downstream patch does lead to a longer recovery length compared to the denser patches. A possible explanation for this phenomenon is that the patches are close enough together to interact with each other, but are far enough apart that the wakes mainly mix with the jet stream created in between the two patches. This jet stream of enhanced velocities in between the patches is then responsible for the fast flow recovery. This is in line with the findings by de Lima et al. (2015), who found that patches placed at T<3D will have an interaction with each other.

The transverse profile of the longitudinal flow velocities is shown in Figure 4.11. Similar to Figure 4.8, the sparse downstream patch shows a skewed profile and the velocities in the wake of the downstream patch are lower for a denser downstream patch, but higher in the wake of the corresponding upstream patch.

The plot of the TKE profile, Figure 4.12, shows the same fast recovery as the velocity profile. Similar to patches that are placed closer together (Figure 4.9), a denser downstream patch results in a higher turbulence peak that is placed further upstream. By comparing the influence of different patch distances for a downstream patch of ϕ=14%, shown in Figures 4.13 and 4.14, it becomes clear that the turbulence peak for a larger T/D is smaller and located more downstream. It is expected that this lower turbulence level is related to a milder velocity gradient, however this is not seen in

Figure 4.15.

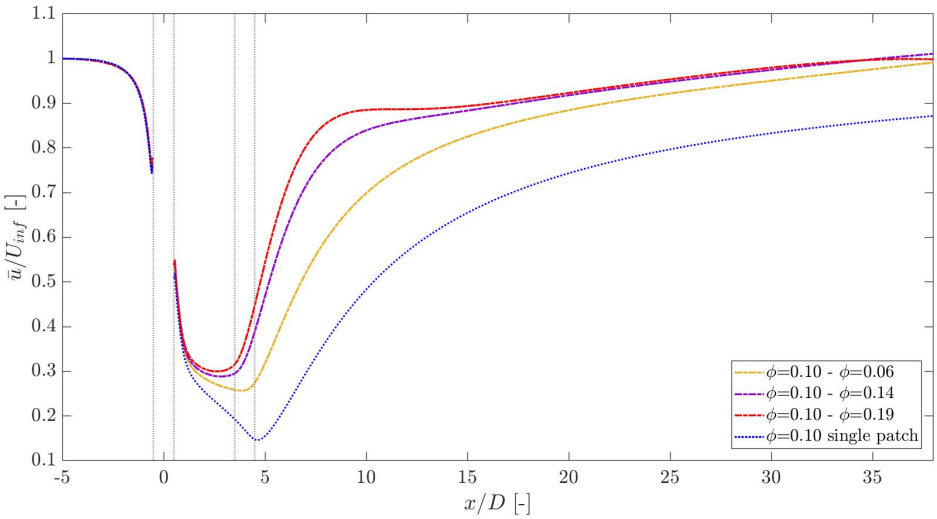

Figure 4.10: Normalized longitudinal velocity profile through the centerline of the upstream patch as it is affected by a downstream vegetation patch with a different density. The grey lines show the location of the upstream patch and the downstream patch, with L=4D and T=2.5D. The legend shows the density ϕ of the upstream patch, followed by the density of the downstream patch.

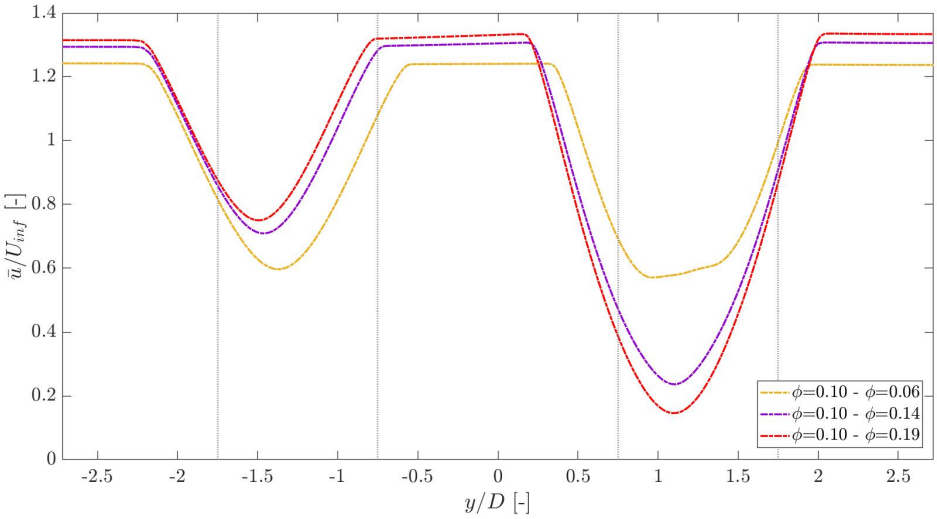

Figure 4.11: Transverse profiles of the longitudinal flow velocities measured at a distance of 4.5D behind the downstream patch, with interpatch distances of L=4D and T=2.5D. The grey lines show where the patches are placed, the two left lines represent the upstream patch and the two right lines represent the downstream patch. The legend gives first the density ϕ of the upstream patch and then the density ϕ of the downstream patch.

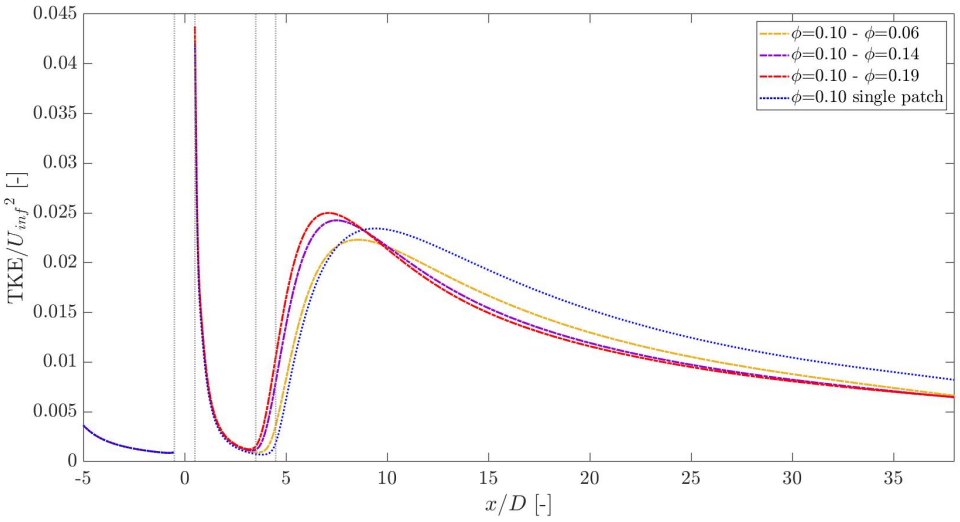

Figure 4.12: TKE profile through the centerline of the upstream patch as it is affected by a downstream vegetation patch with a different density. The grey lines show the location of the upstream patch and the downstream patch, with L=4D and T=2.5D. The legend shows the density ϕ of the upstream patch, followed by the density of the downstream patch.

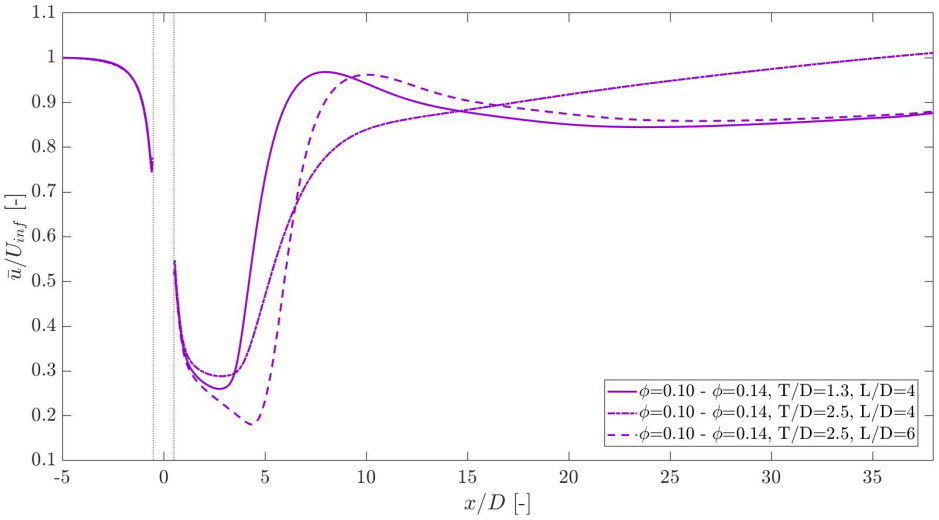

Figure 4.13: Normalized velocity profile through the centerline of the upstream patch as it is affected by a downstream vegetation patch with a different distance. The grey lines show the location of the upstream patch. The legend shows the density ϕ of the upstream patch, followed by the density of the downstream patch.

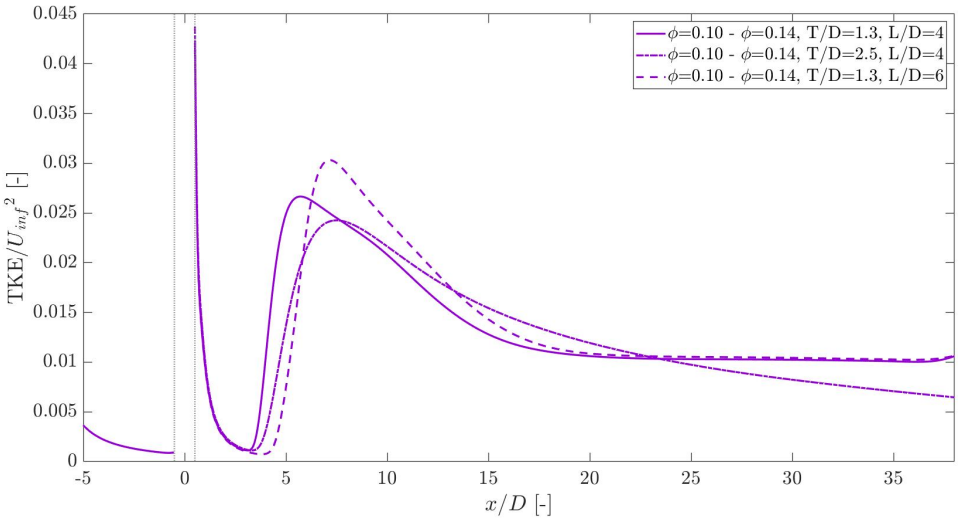

Figure 4.14: Normalized TKE profile through the centerline of the upstream patch as it is affected by a downstream vegetation patch with a different distance. The grey lines show the location of the upstream patch. The legend shows the density ϕ of the upstream patch, followed by the density of the downstream patch.

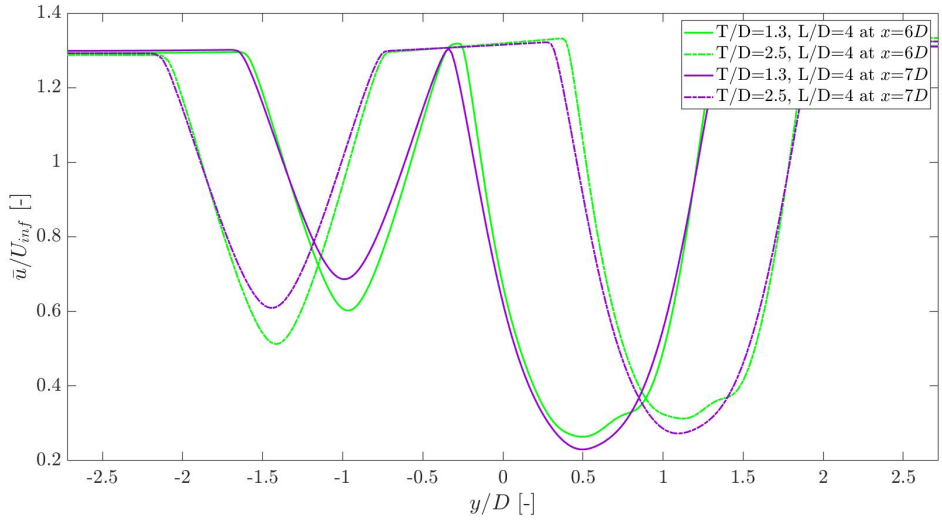

Figure 4.15: Transverse profiles of the longitudinal flow velocities measured at a distance of $2D$ and $3D$ behind the centre of the downstream patch. The profiles show the same patch pair with the upstream patch of ϕ=10% (left) and a downstream patch of ϕ=14% (right) for two different interpatch distances.

For the last comparison with different downstream patch densities, the two patches are laterally placed close together (T=1.3D), but placed further apart in the longitudinal direction (L=6D). The results are shown in Figures 4.16 and 4.17. It can be seen that the shapes of the profiles are very similar to the profiles of the plots for L=4D (Figures 4.7 and 4.9), although the peaks have moved further downstream. The velocity peak shifts about $2D$ downstream and the TKE peak about $1.6D$, which is consistent with the placement of the downstream vegetation patch. The difference between the length of the steady wake behind an upstream patch for a sparser or denser downstream patch is much smaller compared to patches placed at L=4D. This is because the steady wake behind

a patch of ϕ=10% is always the same, but only differs due to the influence of a denser or sparser downstream patch. When this patch is placed much further downstream, the steady wake length behind the upstream patch is already almost at its end before the presence of a downstream patch interferes. Therefore a downstream patch of different density has less effect on the steady wake length for patches placed further apart in the longitudinal direction. In the wake recovery (beyond x=5D), the wake of the upstream patch is affected by the density of the downstream patch. A denser downstream patch leads to higher flow velocities and a sparser downstream patch results in lower flow velocities in the wake recovery.

The TKE profile follows the same trend, where the denser downstream patch generates a larger peak in the wake of the upstream patch than a sparser patch. Interesting is that the peaks for both densities are much higher compared to the TKE peaks of patches placed at L=4D, which also becomes clear from Figure 4.14. This is the result of the fact that the velocity in the steady wake behind the upstream patch is lower where the downstream patch is located. As nothing else is altered about the downstream patch, the flow diversion around this patch is still the same, resulting in a similar jet stream between the patches as when they are placed closer together. Due to the lower velocity in the steady wake, the velocity gradient between the two flows is steeper and therefore results in higher turbulence levels.

The transverse profile of the longitudinal velocities, shown in Figure 4.18, is not much different from the transverse profile in which the patches are placed at L=4D (Figure 4.8). Again, a denser downstream patch generates lower velocities in the wake of the downstream patch, but higher velocities in the wake of the upstream patch due to the flow diversion and intense mixing.

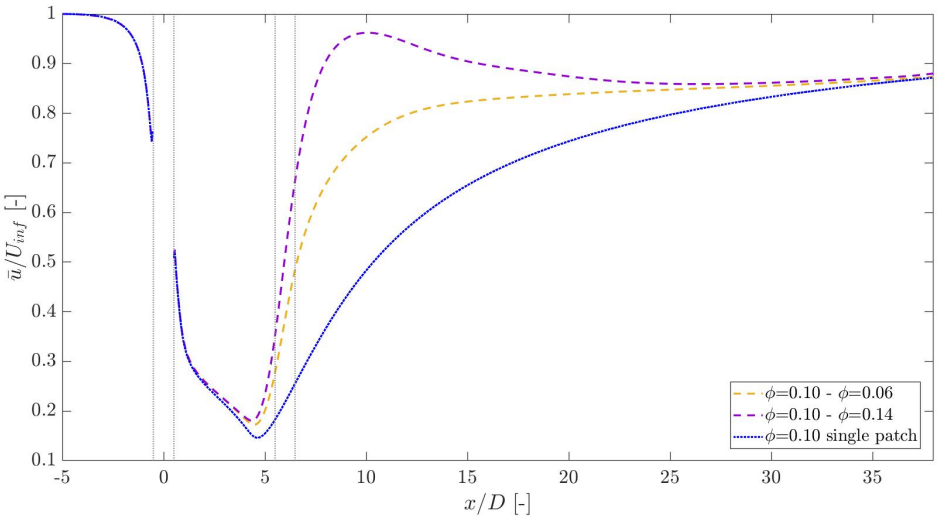

Figure 4.16: Normalized velocity profile through the centerline of the upstream patch as it is affected by a downstream vegetation patch with a different density. The grey lines show the location of the upstream patch and the downstream patch, with L=6D and T=1.3D. The legend shows the density ϕ of the upstream patch, followed by the density of the downstream patch.

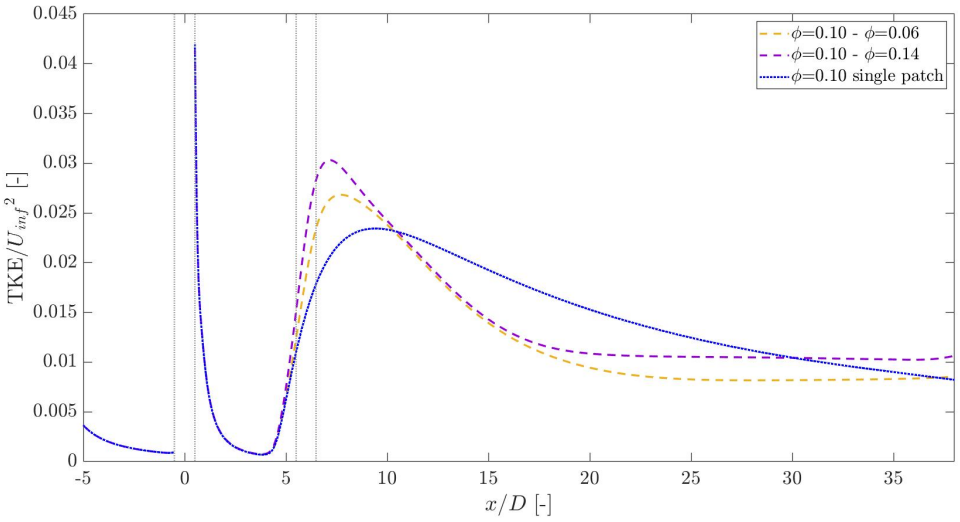

Figure 4.17: Normalized TKE profile through the centerline of the upstream patch as it is affected by a downstream vegetation patch with a different density. The grey lines show the location of the upstream patch and the downstream patch, with L=6D and T=1.3D. The legend shows the density ϕ of the upstream patch, followed by the density of the downstream patch.

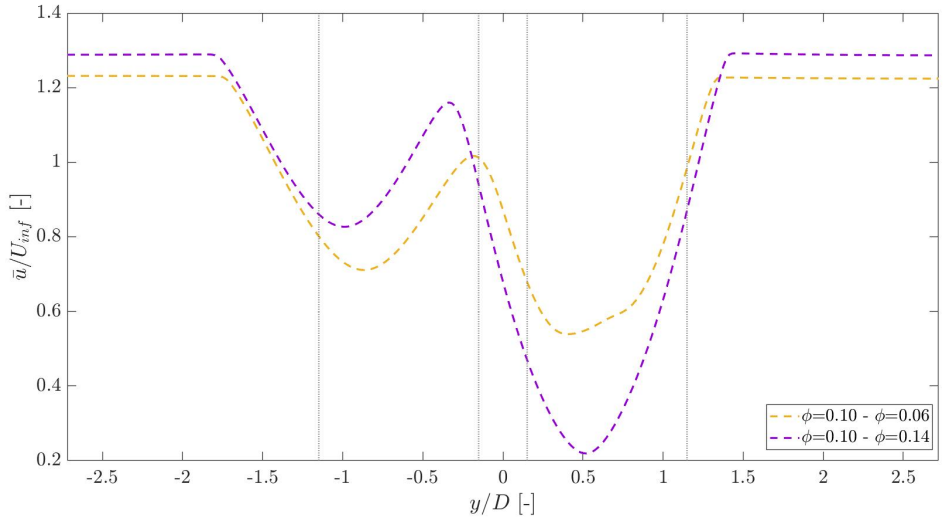

Figure 4.18: Transverse profile of the normalized longitudinal flow velocities measured at a distance of 4.5D behind the downstream patch, with interpatch distances of L=6D and T=1.3D. The grey lines show where the patches are placed, the two left lines represent the upstream patch and the two right lines represent the downstream patch. The legend gives first the density ϕ of the upstream patch and then the density ϕ of the downstream patch.

4.2.2 Influence on downstream patch

Contrary to the wakes behind the upstream patches, the velocity in the wake behind a downstream patch is not as much influenced by the density of an upstream patch. As seen in Figure 4.19, the steady wake length barely differs between different patch combinations. Even compared with a single patch, there is no significant influence. In front of the downstream patch, on the other hand, an increase in velocity takes place. This velocity peak is larger for a denser upstream patch,

but occurs for a much sparser upstream patch as well. The increase of velocity in this location is related to the flow diverting around the upstream patch, which results in flow acceleration around the sides of the upstream patch. These enhanced flow velocities mix with the flow approaching the downstream patch, and result in such peaks. Larger peaks are a result of larger flow acceleration around denser upstream patches.

The transverse velocity profile of normalized longitudinal velocities, which can be seen in Figure 4.20, shows these increased velocities on the sides of the wakes of both patches for a denser upstream patch. Overall, the transverse profile is not affected much by a different density of the upstream patch. The odd shape of the velocity profile in the wake of the sparse patch that is seen in Figure 4.8, is no longer present when the sparse patch is the upstream patch. For this transverse profile, the velocities for the sparser patches are measured much further downstream and the individual streams of lower and higher velocity that exit the sparser patches have had time to mix.

The TKE profile in Figure 4.21 shows that a denser upstream patch results in a higher turbulence level in the wake of the downstream patch. Directly behind the downstream patch, there is a peak in TKE, which is caused by the stem-generated turbulence. This only occurs on small length-scales and the turbulence level drops down to a minimum in the steady wake region. At the end of the steady wake region behind the downstream patch, the turbulence level spikes to a maximum when shear layers meet each other and the Von Karman vortex street sets off. The fact that a denser upstream vegetation patch generates the highest TKE peaks is due to the higher velocity peak upstream of the downstream patch and the enhanced flow velocities on the side of the patch. Such high velocities result in a steeper velocity gradient which induces more turbulence.

These findings correspond mostly with the findings by Kitsikoudis et al. (2020). A denser upstream patch results in a slightly shorter steady wake length and in a higher TKE peak. A significant difference is that their findings suggest that a denser upstream patch results in a TKE peak that is more upstream than the peak for a sparser upstream patch. This is not the case for this study, as the turbulence peaks do not seem to change much in location for a sparser or denser upstream patch, or even for an individual patch.

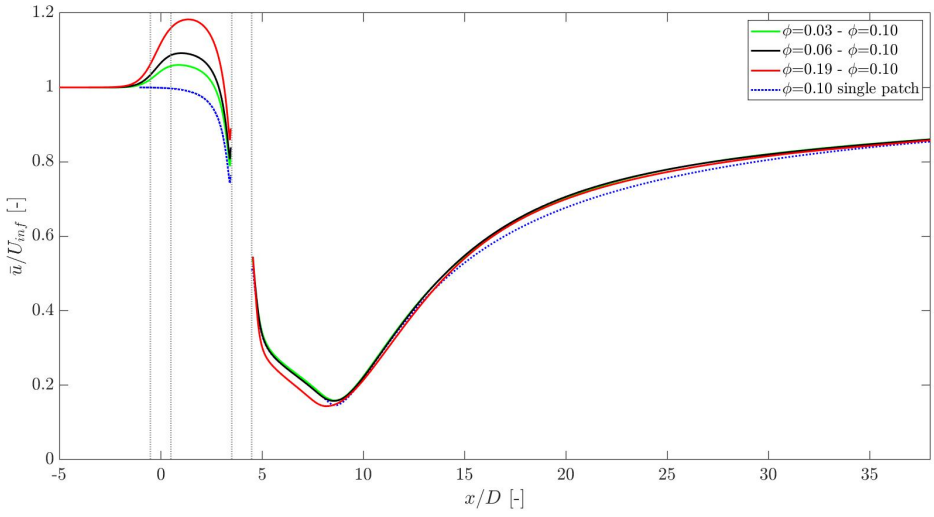

Figure 4.19: Normalized velocity profile through the centerline of the downstream patch as it is affected by an upstream vegetation patch with a different density. The interpatch distances are L=4D and T=1.3D. The downstream patch is located between 3.5D and 4.5D. The legend shows the density ϕ of the upstream patch, followed by the density of the downstream patch.

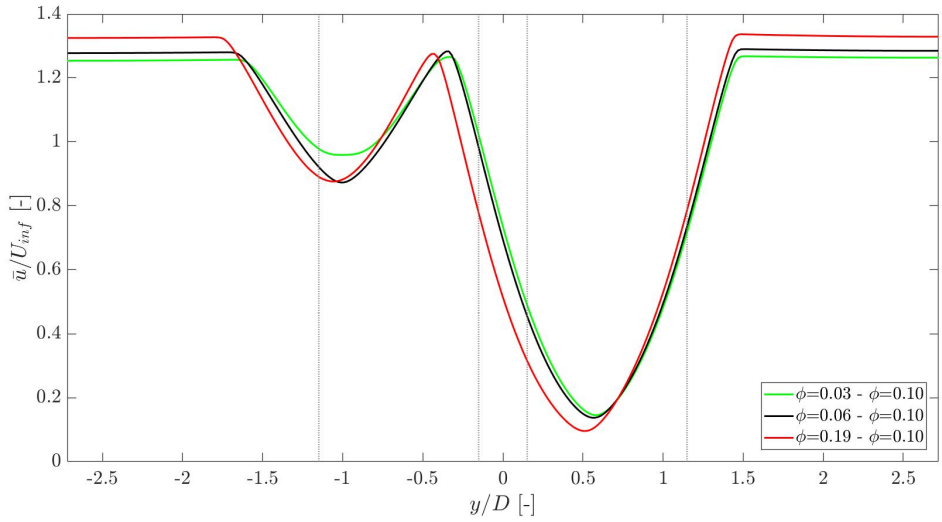

Figure 4.20: Transverse profile of the normalized longitudinal velocities measured at $4.5D$ behind the downstream patch. The grey lines show where the patches are placed, the left lines represent the upstream patch and the right lines represent the downstream patch. The interpatch distances are L=$4D$ and T=$1.3D$. The legend gives first the density ϕ of the upstream patch and then the density ϕ of the downstream patch.

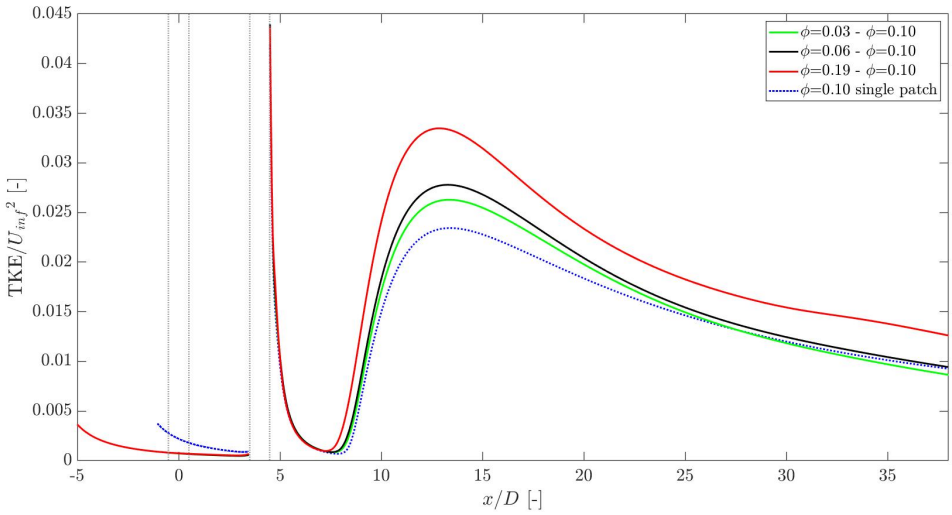

Figure 4.21: Normalized TKE profile through the centerline of the downstream patch as it is affected by an upstream vegetation patch with a different density. The interpatch distances are L=$4D$ and T=$1.3D$. The downstream patch is located between $3.5D$ and $4.5D$. The legend shows the density ϕ of the upstream patch, followed by the density of the downstream patch.

4.2.3 Wake merger

Figures 4.22 and 4.23 show the progression of the wakes behind two vegetation patches compared to the wake behind a single vegetation patch. From both figures, it becomes clear that at $24D$ behind the downstream patch, the wakes have merged and propagate through the flow domain as a single wake. This is in line with the findings by Meire et al. (2014), who found that wake merger also occurred for two patches placed side-by-side.

Figure 4.23 shows that the transverse profile of the wake of the downstream patch is very similar to the profile of an individual patch with the same characteristics, placed and measured at the same locations. Figure 4.22, where the same is done but for an upstream patch, shows less coherence between the wake of an upstream patch and a corresponding individual patch. This indicates that the wake of a downstream patch is much less affected by the presence of an upstream patch than vice versa.

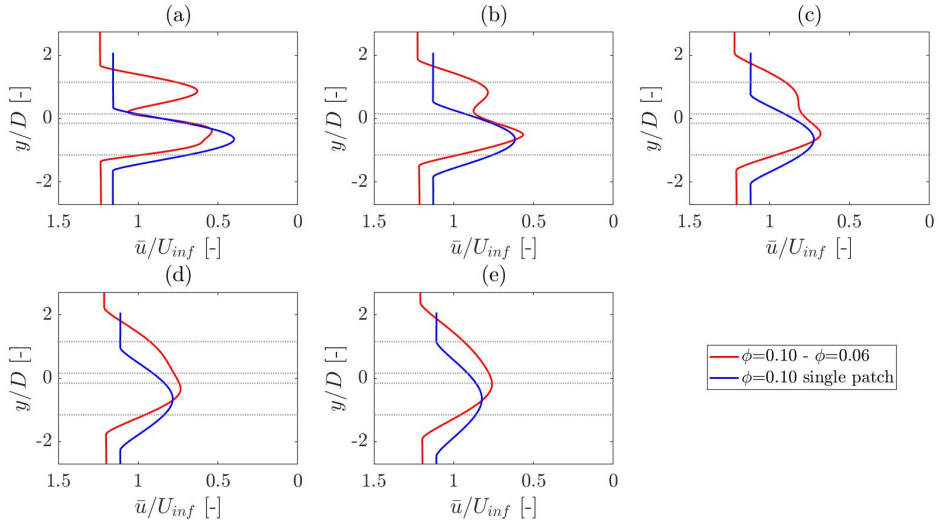

Figure 4.22: Evolution of the transverse profile of normalized longitudinal flow velocities measured at $4D$ (a), $9D$ (b), $14D$ (c), $19D$ (d) and $24D$ behind the downstream patch. The two grey lines at the top of each figure represent the downstream patch with a density of ϕ=6%, and the two grey lines at the bottom of each figure represent the upstream patch with a density of ϕ=10%. The interpatch distances are L=$4D$ and T=$1.3D$.

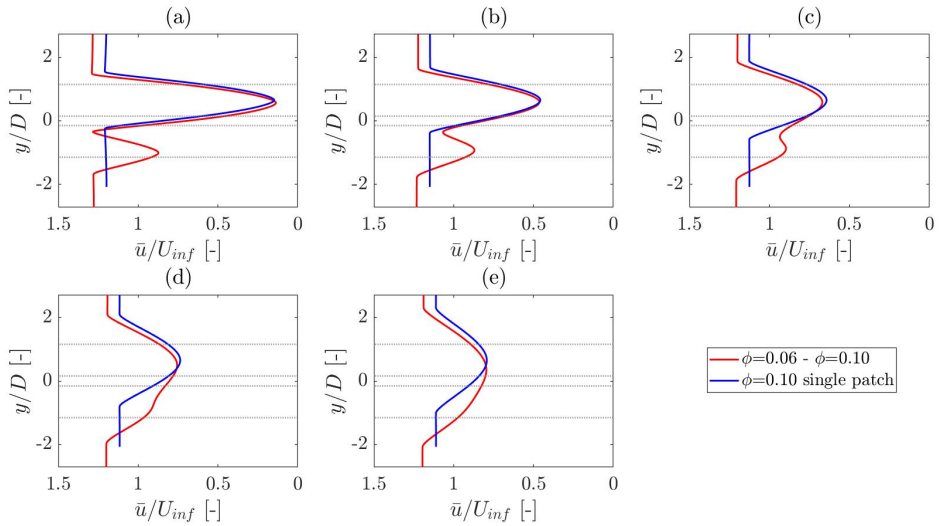

Figure 4.23: Evolution of the transverse profile of normalized longitudinal flow velocities measured at $4D$ (a), $9D$ (b), $14D$ (c), $19D$ (d) and $24D$ behind the downstream patch. The two grey lines at the top of each figure represent the downstream patch with a density of ϕ=10%, and the two grey lines at the bottom of each figure represent the upstream patch with a density of ϕ=6%. The interpatch distances are L=$4D$ and T=$1.3D$.

4.3 Sediment transport and deposition

For every run performed in Section 4.2, an analysis was made on how much enhanced sediment transport and deposition could potentially be generated by a specific model setup for patches with different densities. Two methods are used to calculate this percentage, the first is called the velocity and TKE method (V+TKE) and the second is called the velocity threshold method (VT0.7), which are explained in more detail in Section 3.3. The results for each run are shown in Table 4.1. This table shows the percentage of the total model domain where enhanced sediment deposition could take place and potentially lead to new vegetation growth.

Table 4.1: All runs with corresponding patch densities and the results on the two methods for the analysis of enhanced sediment deposition.

Run	Density upstream [-]	Density downstream [-]	V+TKE	VT0.7
1	0.10	0.03	5.57%	4.00%
2	0.10	0.06	1.36%	7.24%
5	0.10	0.14	0.60%	8.10%
6	0.10	0.19	0.53%	7.89%
7	0.10	0.06	1.35%	7.29%
8	0.10	0.14	0.60%	8.02%
9	0.10	0.19	0.53%	7.99%
10	0.10	0.06	1.41%	7.47%
11	0.10	0.14	0.72%	8.58%
12	0.03	0.10	5.53%	6.47%
13	0.06	0.10	1.42%	7.36%
14	0.19	0.10	0.69%	8.91%

The results for the velocity threshold method present some inconsistencies, although there seems to be a trend that a run with a sparser neighbouring patch results in a lower percentage of enhanced sediment deposition. This is in line with the findings by Yamasaki et al. (2019), where patches that represented a lower flow blockage resulted in less initial vegetation growth.

The velocity and TKE method gave the opposite results. Under these conditions, the area of enhanced sediment deposition grows for sparser patches, instead of becoming smaller. The calculated percentages remain unchanged for variations in interpatch distance, which is not always the case for the velocity threshold method. The findings for the velocity and TKE method are in line with the findings by Ortiz et al. (2013), who suggest that sparser patches may result in a larger area of enhanced sediment deposition due to the increased length of the steady wake regions and reduced TKE.

The contradiction of the two methods raises a problem, which is further evaluated by looking at the location of deposition patterns, shown in Figures 4.24a and 4.24b for run 2 and Figures 4.25a and 4.25b for run 5. The top frame shows the results for the velocity and TKE method and the bottom frame shows the velocity threshold method. Deposition patterns for the other runs can be found in Appendix B.2. It is important to keep in mind that figures such as Figures 4.24a and 4.24b only show the locations where enhanced sediment deposition could take place, and do not elaborate on the magnitude of deposition. The construction of this figure implies that sediment deposition is the same in all locations, however this could just be a few grains in some locations, but a more substantial amount in other locations.

The velocity threshold method (Figure 4.24b) shows a lot more sediment deposition in the wake of both patches compared to the velocity and TKE method (Figure 4.24a). According to the experimental research by Chen et al. (2012), sediment deposition patterns exceeding the length of the steady wake region are unlikely, as the increasing turbulence associated with the end of the

steady wake region keeps sediment in motion. This means that for this reason, the deposition pattern with the velocity and TKE method should be closer to reality. Comparing Figure 4.24a to Figure 4.7 shows that the sediment deposition behind the upstream patch roughly stops as the steady wake region ends. The gap between the patch and area of enhanced sediment deposition is explained by the presence of stem-scale turbulence generated by the stems closest to the back of the vegetation patch (Chen et al. 2012; Chang and Constantinescu 2015). This increased turbulence is also visible in Figure 4.9, around x/D=0.5 - 1.

With the velocity threshold method, a lot of sediment deposition is simulated between the stems. This is caused by the fact that the effect of turbulence on sediment deposition is not taken into account, and this method therefore overlooks the effect of the stem-scale turbulence. The experimental study by Yagci et al. (2017) shows that there is no enhanced sediment deposition in between the patch, as there is mainly a pattern of scour around each individual stem.

Comparing Figure 4.24a against Figure 4.25a gives a further insight in the effect of a downstream patch with different density on the sediment deposition pattern as determined with the velocity and TKE method. From Table 4.1, it becomes clear that patch combinations with a smaller density result in a larger area of enhanced sediment deposition. This is also visible from the figures, as there is a larger area of enhanced sediment deposition behind the sparser downstream patch compared to the denser downstream patch. As described in Section 1.1, sparser patches generate lower turbulence levels, which explains why the area of enhanced sediment deposition is larger behind a sparser downstream patch. The sediment deposition pattern behind the upstream patch is not affected much by the presence of a denser or sparser downstream patch.

Comparing Figure 4.24b against Figure 4.25b gives further insight in the different deposition patterns that result from the velocity threshold method for a varying density of the downstream patch. Here, the deposition pattern behind both the upstream and the downstream patch is affected for a denser or sparser downstream patch. For a denser downstream patch, the area of enhanced sediment deposition behind the downstream patch increases, and decreases behind the upstream patch. As described in Section 1.1, a denser downstream patch results in a lower flow velocity in its wake, which then also provides more area for sediment deposition. Flow diverting around a denser downstream patch has a larger effect on the wake of the upstream patch, as mentioned in Section 4.2.1. This results in higher flow velocities in the wake of the upstream patch (Figure 4.7), and thus less area with potential for sediment deposition and consequently vegetation growth.

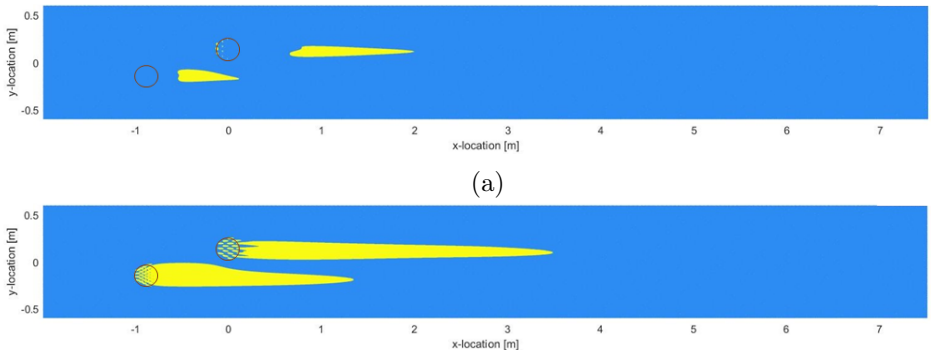

(a)

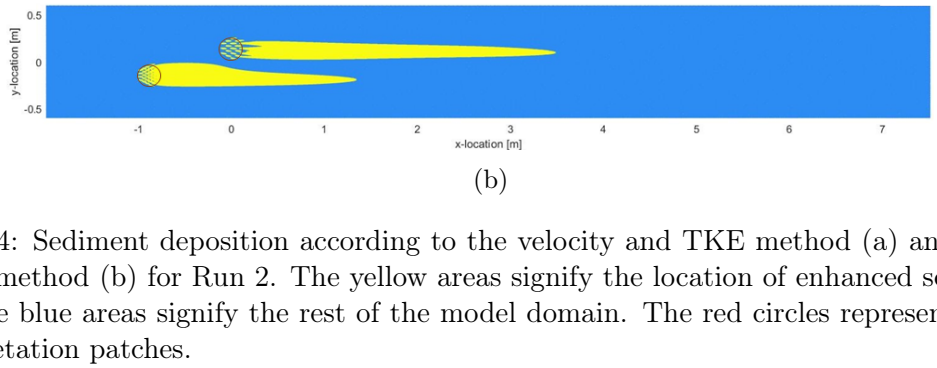

(b)

Figure 4.24: Sediment deposition according to the velocity and TKE method (a) and the velocity threshold method (b) for Run 2. The yellow areas signify the location of enhanced sediment deposition. The blue areas signify the rest of the model domain. The red circles represent the outlines of the vegetation patches.

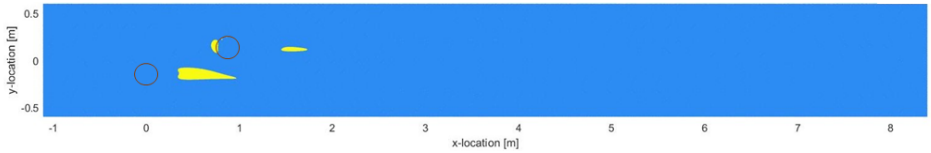

(a)

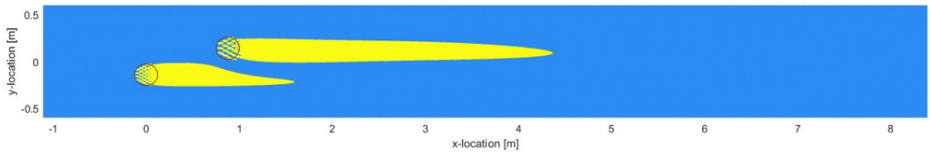

(b)

Figure 4.25: Sediment deposition according to the velocity and TKE method (a) and the velocity threshold method (b) for Run 5. The yellow areas signify the location of enhanced sediment deposition. The blue areas signify the rest of the model domain. The red circles represent the outlines of the vegetation patches.

Comparing Figure 4.24a with 4.26a gives further insight in the sediment deposition patterns generated by the velocity and TKE method, when the upstream patch changes in density. The area of the deposition pattern behind the upstream patch increases for a sparser upstream patch, similar to the areas behind the downstream patches in Figures 4.24a and 4.25a. The downstream patch is not affected much by a varying density of the upstream patch. The small difference that is present between the two scenarios is the result of a lower TKE value in the wake the downstream patch with a sparser upstream patch, shown in Figure 4.21.

To analyse the influence of an upstream patch of different density with the velocity threshold method, Figures 4.26b and 4.27b are compared against each other. With an upstream patch of varying density, the sediment deposition pattern behind the downstream patch barely changes. This is due to the fact that the velocity in the wake of a downstream patch is not significantly affected by the presence of a downstream patch of different density, as described in Section 4.2.2 and visible in Figure 4.19. The sediment deposition pattern behind the upstream patch increases with increasing density, which is caused by the reduced velocities in the wake of a denser patch, as described previously.

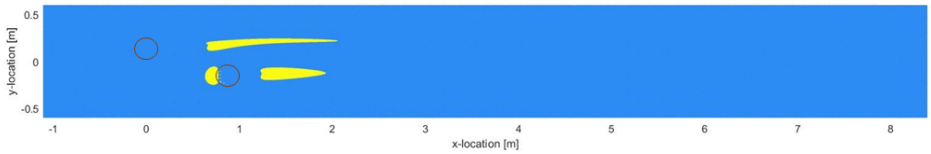

(a)

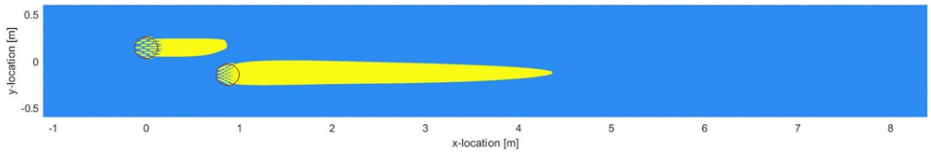

(b)

Figure 4.26: Sediment deposition according to the velocity and TKE method (a) and the velocity threshold method (b) for Run 13. The yellow areas signify the location of enhanced sediment deposition. The blue areas signify the rest of the model domain. The red circles represent the outlines of the vegetation patches.

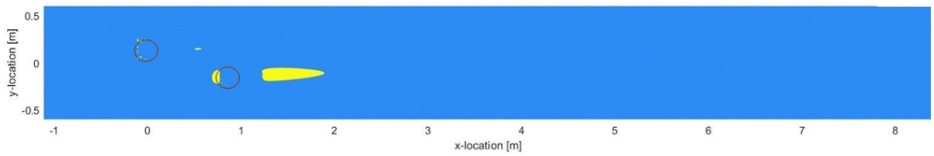

(a)

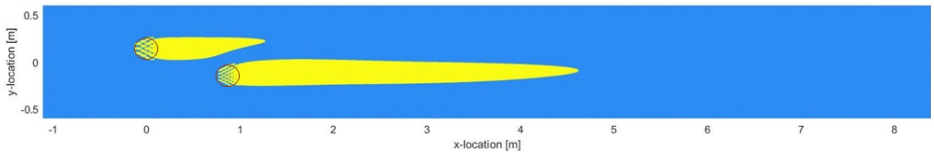

(b)

Figure 4.27: Sediment deposition according to the velocity and TKE method (a) and the velocity threshold method (b) for Run 14. The yellow areas signify the location of enhanced sediment deposition. The blue areas signify the rest of the model domain. The red circles represent the outlines of the vegetation patches.

Something that has been mentioned briefly above is the influence of the interpatch distances and location on the area of enhanced sediment deposition. These differences are incredibly small for the velocity and TKE method, often smaller than 0.1% (Table 4.1), which suggests that the growth of new vegetation is independent of the location of the two original patches. With the velocity threshold method, a small increase in area of enhanced sediment deposition is observed for an interpatch distance of L=6D instead of L=4D (runs 10 and 11 in Table 4.1). A reason for this is that the steady wake length behind the upstream patches in this scenario is longer, as seen in Figure 4.13. This results in more favourable conditions for sediment deposition behind the upstream patch and increases the total area of enhanced sediment deposition.

Table 4.1 also shows two instances for an increase in enhanced sediment deposition resulting from a difference in upstream or downstream placement of a patch. When the upstream patch is the denser patch of ϕ=19% (Figure 4.27b), the total amount of potential sediment deposition is increased a significant amount compared to when this denser patch is placed in a downstream location. Behind a denser patch, enhanced sediment deposition takes place over a shorter distance due to the shorter steady wake length. When this denser patch is placed upstream, it does not disturb the wake of the downstream patch of ϕ=10%, which generates more enhanced sediment deposition. If the denser patch is placed downstream, it interferes with the wake of the sparser patch, which results in the decreased amount of enhanced sediment deposition and thus potential vegetation.

When the upstream patch is the sparse patch of ϕ=3%, the amount of potential sediment deposition is also significantly increased compared to when the sparser patch is placed at a downstream position. Looking at figures of the enhanced sediment deposition patterns, Figures B.13b and B.22b in Appendix B.2, it is clear that the velocity in the wake of the sparse patch is barely low enough for sediment deposition according to the velocity threshold method. This is also the case when the sparse patch is placed at the downstream location. This means that the main area of sediment deposition is in the wake of the patch with ϕ=10%. The difference in area occurs because, when placed upstream, the presence of the sparse patch does not interfere with the wake of its neighbouring patch. When the sparser patch is placed downstream, it interferes with the wake of the upstream patch, increasing the flow velocity and resulting in less enhanced sediment deposition. This is however only the case for the sparsest patch, as placing a patch of ϕ=6% upstream or downstream does not result in a significant difference.

Despite these few examples for different sediment deposition patterns resulting from placing the patches at different locations, the most prominent variations in deposition patterns are still a result of density differences between patch combinations. This is the case for both methods. The

amount of new vegetation growth is then much more dependent on the total flow blockage that a patch combination represents, than the distance between these two patches. Both methods also predict that the most significant deposition pattern is behind each of the two patches, and that a secondary deposition zone does not occur for the evaluated scenarios. This means that the original two patches both can expand in the longitudinal direction, as Yamasaki et al. (2019) also found, however patch merger is unlikely due to the absence of the secondary deposition zone.

5 Discussion

5.1 Model limitations and validation data

As this research had to be completed within a set time limit, certain choices have been made that were motivated by this limitation. The first was the choice of the model. As explained in section 1.1, a RANS model is only accurate until a certain level and is not suitable to accurately compute the adverse pressure gradient and flow separation caused by a vegetation patch. A RANS model in combination with a $k-\omega$ turbulence closure model would be able to compute this, however it was found that such models did not converge in this case. This was likely due to the fact that a partially unsteady flow was modelled with a steady flow simulation. By only calculating the time-averaged velocity and TKE, the model is unable to capture unsteady characteristics such as vortex shedding or a von Kármán vortex street. However, as de Lima et al. (2015) pointed out, a RANS model is able to reproduce the most significant characteristics of a steady wake. A more accurate method would be the Large Eddy Simulation (LES), although a much finer grid is required which already increases computational time. On top of that, LES models need a long running time to generate stable statistics on the flow behaviour. Instead of using turbulence closure models to model the largest eddies, as RANS models do, LES computes these eddies directly and only models the smallest eddies. Small eddies are more isotropic and universal compared to large eddies, which makes it possible to apply a turbulence model that matches the physics of all small eddies (Ye et al., 2021). With the implementation of a LES model, the calculated TKE could have been much more precise, which could have given a better insight on locations where enhanced sediment deposition takes place. However, for the purpose of this research, a RANS model is sufficient to obtain an initial grasp of the effect that patches with different densities have on the flow.

Choosing to use a RANS model instead of a more precise turbulence model is one of the main model simplifications that can lead to uncertainties in the results. Another simplification is made by selecting rigid cylinders to represent the vegetation stems. These cylinders are completely smooth and will continue to stand upright in the same position for all model conditions. In reality, even the most rigid type of vegetation will experience some form of oscillation due to the flow passing by it. Furthermore, all vegetation carries leaves that will create an additional drag on the flow (Schnauder and Moggridge, 2009). By choosing such smooth, stiff cylinders, smaller effects are not taken into account that could each have an additional effect on the flow and influence the velocity and turbulence levels generated by the patch.

The first choice for the CFD modelling tool with RANS equations was the program OpenFOAM. However, when performing test runs, model convergence was not achieved. Therefore, the choice was made to switch to a different CFD modelling tool, which was Ansys Student 2022 R1 with the solver Fluent. Where in OpenFOAM it is easy to place stems, change their location and alter the dimensions when necessary, this is not the case for FLUENT®. Setting up the model in FLUENT® takes much more time compared to OpenFOAM, which put a limit on the amount of runs that could be performed. This meant a limit on the runs of the actual research, but also on the amount of runs for the model validation. As described in section 4.1.2, a choice had to be made early on to continue with the circular patch, even though there was a possibility that the square patch might have ended up being a better fit with wall functions that were not tested. However, the patch type that was chosen despite these limitations, fits the validation data reasonably well. Therefore the results produced with this type of patch are still valid. On top of that, the focus of this research was not on the exact values produced with the model, but on the differences between different scenarios. As all scenarios are run with the same model, the deviation is the same for each scenario which cancel each other out.

Other uncertainties were introduced by limitations in the published validation data. The transverse profile of the longitudinal velocity from Zong and Nepf (2011) that was used for the validation data (Figure 4.3) only extends up to y=2D, whereas the outer wall is located at y=2.7D. It is there-

fore unclear if the velocity continues to reduce after point y=2D, which would mean that the outer wall has a large impact on the flow domain. Another scenario could be that the velocity remains around u/U_{inf}=1, and reduces much closer to the wall, which would mean that drag caused by the outer wall has less impact on the flow. This last scenario would also imply that the reference model is better at simulating the drag of the wall than that is now estimated. Furthermore, no information was published on the turbulent kinetic energy present around the validation patch. The amount at which the model is able to predict the TKE in the model domain is therefore not examined. This means that no statement can be made on the accuracy of the TKE profiles in section 4.2.

5.2 Model output

With the way that FLUENT® works, it was easiest to create a circular patch with 7, 19, 37 or 61 stems. This is a result of the structured grid, which works with a specific amount of cells in the x- and y-direction, which cannot change throughout the model domain. This has an influence on the way that finer grid cells are placed around the cylinders. In order to do this, a square had to be formed manually around each cylinder, which gives a limitation in the amount of stems that can be used in order to still keep the patch circular. The setup of a square patch allowed a few more options: 4, 9, 16, 25, 36 and 49. For the model validation, this meant that the amount of stems and the dimensions used by Zong and Nepf (2012) could not exactly be replicated. Considering the cell limit, a patch with 61 stems was never used, and neither was a patch of 7 stems, because they were not considered to be representative. This could have been the reason that the best suitable model still had a maximum velocity difference of 11%. With a different amount of stems that have a different diameter, the flow diversion that occurs around each stem is different and will affect the properties of the flow. However, de Lima et al. (2015) used a square vegetation patch with 35 stems to validate their model in FLUENT® and the maximum difference they found was 6%. Therefore the conclusion was reached that the 11% difference was either caused by another difference in model choices, or at least a combination of the limited number of stems and other model choices.

According to the experimental studies performed by Meire et al. (2014) and Rominger and Nepf (2011), the upstream adjustment length in front of a patch scales to the diameter of that patch and is independent of the patch density. Although this is not the focus of this research, it is found that this is not the case when comparing Figures 4.5 and 4.7. The upstream adjustment length, L_0, for a patch of ϕ=3% is found to be 3D. The L_0 for a patch of ϕ=10% seems to be 4.4D, although this cannot be evaluated for certain as the model domain does not extend further than 4.5D in front of the patch. Alternatively to Rominger and Nepf (2011) and Meire et al. (2014), Chen et al. (2012) proposes a scale factor which implies that patches with a higher density result in a longer adjustment length than sparser patches. This corresponds with the findings of this study.

The specific reasons for why the $k-\omega$ SST turbulence closure model did not lead to convergence for the reference case are not exactly known. It would have been interesting to see if this model would have resulted in improved validation simulations. As the model is known for providing more accurate results in the boundary layer compared to the $k-\epsilon$ model, due to the employment of the standard $k-\omega$ model, it could have resulted in a better-fitting transverse velocity profile, compared to the profiles already shown in Figure 4.3 (Durbin, 2004). Another factor that plays a role here is that the $k-\omega$ SST model performs best when the y^+ value near the sidewalls and the walls of the individual stems is lower than 5, whereas most wall functions of the $k-\epsilon$ model give the best results for y^+>30. Due to necessary grid cell refinement around the stems, a y^+ value of larger than 30 is nearly impossible. As a y^+ value between 5 and 30 is undesirable, it was decided that a value lower than 5 would be used for the individual stems of the vegetation patches (ANSYS Inc., 2014). For these model settings, a $k-\omega$ SST model might have simulated more realistic velocities.

Various other runs with the RNG $k-\epsilon$ model did not converge either. These were runs with a downstream patch of densities between ϕ=8% and ϕ=12%. It is remarkable that these runs did not converge, although a reason for it has not yet been found. If would have been interesting to

investigate the influence of even more different patch densities, however the runs that are performed in this research already give a good idea on the influence of a sparser or denser neighbouring patch.

A limiting factor for the results with two staggered patches was the maximum amount of cells that the Ansys Student version allows. This consequently meant that it was not possible to use a large number of stems, as more stems would result in more grid cells to get the right refinement. This played a small role in the results of the model validation, but mainly influenced the model setup for the two staggered patches. As explained in section 4.2, it was not possible to have two patches with each 37 stems. As seen from Figures 4.2 and 4.3, a patch with 19 stems generates significantly worse results than its counterpart with 37 stems. Using this configuration for the neighbouring patch could have a large effect on the accuracy of the steady wake length and flow velocity behind this patch. Therefore the focus was only on the wake of the patch with 37 stems. A neighbouring patch with only 19 stems will cause a different effect than a neighbouring patch with 37 stems, meaning that this choice could have had an impact on all results in section 4.2.

For a downstream patch of different density, four different densities were evaluated (ϕ=3%, ϕ=6%, ϕ=14% and ϕ=19%). On top of that, the influence of different distances was also explored, which were the following: L=4D and T=1.3D, L=4D and T=2.5D, and L=6D and T=1.3D. For an upstream patch of different density only the interpatch distances of L=4D and T=1.3D were tested. By comparing the velocity and TKE profiles in the wake of a downstream patch with a different upstream density (Figures 4.19 and 4.21) to profiles in the wake of an upstream patch with a downstream patch of different density (Figures 4.7 and 4.9), it becomes clear that changing the latter has a much larger effect on the shape and quantities of the velocity and TKE profiles. This validates the choice made in Section 3.2, to perform more runs with a downstream patch of different density than an upstream patch of different density. Nonetheless, there are still significant differences between upstream patches of different densities that are worth exploring.

By removing part of the data in front of the patch, as mentioned in Section 3.3, the opportunity to explore enhanced sediment deposition in front of the patch is also eliminated. For example, from experimental research, both Zong and Nepf (2010) and Meire et al. (2014) noticed enhanced deposition upstream of the patch. This deposition was equal to the upstream adjustment length. Zong and Nepf (2010) used patches of densities ϕ=2% and ϕ=10% and Meire et al. (2014) used patches between ϕ=3.3% and ϕ=11%. This enhanced deposition is mainly linked to the reduced flow velocity in front of the patch, which then also reduces the bed stress. On the other hand, both Ortiz et al. (2013) and Chen et al. (2012) did not observe enhanced sediment deposition in front of their sparse patch, as they found that their version of a sparse patch lets enough of the flow through such that the bed stress is not diminished and the TKE does not drop.

Another problem with the velocity and TKE method is that according to Ortiz et al. (2013), erosion also occurs under the given conditions that are used to determine sediment deposition. These conditions are that the velocity and TKE values must be lower than the upstream velocity and TKE values in order for enhanced sediment deposition to take place. Ortiz et al. (2013) found that if enhanced sediment deposition is taking place, it occurs 100% of the time under these conditions. However, they found that in a few instances, erosion can also take place under these conditions, which is then most likely related to other processes. This means that the total area of enhanced sediment deposition is possibly smaller than that is determined in the results in Section 4.3, as some of the area is also prone to erosion. However, the amount of area for which this occurs will be small as erosion mainly tends to occur in regions of high velocity and TKE (Ortiz et al., 2013).

In Section 4.3, it was discussed that a patch with ϕ=3% results in minimal enhanced sediment deposition in its wake for the velocity threshold method. This deposition is significantly smaller than the deposition behind a patch of ϕ=10%, although the opposite would have been expected as a sparser patch generates a longer steady wake length and thus a larger area of diminished flow velocities. It could be that this patch is too sparse to generate a zone of enhanced sediment deposition, however Chen et al. (2012) found in their experiments that a patch of similar density

(ϕ=3.1%) did have a region of enhanced sediment deposition in the wake. This region extends up to $8D$ behind the patch. A more plausible option is that the high velocities in the wake of the sparser patch are caused by the lack of accuracy of a cylinder with only 19 stems. This is also shown in Figure 4.2, where the patches with lesser stems generated significantly higher wake velocities compared to patches with more stems. This is possibly the same reason why the velocity and TKE method generates such large areas for a patch combination in which one of the two has a density of ϕ=3%, as seen in Table 4.1. With the few amount of stems which are relatively small due to the sparseness of the patch, the TKE in the wake of the patch does not spike, but stays consistently low for a long distance. This is shown in Figures B.25 in Appendix B.3.

Meire et al. (2014) and Yamasaki et al. (2021) also found a secondary deposition zone in between the two patches that were placed side-by-side, which is not present in either of the two methods. This secondary deposition zone is related to the merging of the two patch wakes, which results in an area of low flow velocity and turbulence. For a staggered configuration, de Lima et al. (2015) also found a secondary deposition zone for a velocity threshold of 0.7, as long as the patches were placed close enough together in the longitudinal direction (L/D=1). A reason that this secondary deposition zone is not present in this study could be due to the fact that the patches are not placed close enough to each other, as the closest longitudinal distance is $4D$. Important to add is that the research by de Lima et al. (2015) has been performed with the same type of 2D model as used in this study, which means that these findings are not backed up by experimental observations.

The findings of this research can be applied to large-scale applications on a qualitative scale. As this research focuses on the flow patterns created by emergent vegetation, the applicability of these findings is limited to rivers in which this type of vegetation occurs. Nonetheless, this research can provide additional insight in locations of enhanced flow velocities and turbulence levels in rivers. This research also provides two methods which analyse how enhanced sediment deposition can be promoted or diminished, which could be of interest when vegetation growth is of interest or not. With regards to the findings of Yamasaki et al. (2019), who state that vegetation will eventually reach the same amount of coverage, independent of the initial coverage, this research is mostly useful to apply in situations where either slow or quick vegetation growth is necessary. Yamasaki et al. (2019) do not elaborate on the timescales in which the final coverage will occur, however this could take up a long time and the amount of the initial coverage does play a large role in slowing down or speeding up this process.

It is important to realize that vegetation development and growth is not as straightforward as suggested in Section 4.3. The patches used in this research facilitate the growth of new vegetation by creating a positive feedback loop. Enhanced velocities caused by the flow diverting around each patch can result in a negative feedback loop on the sides and on the centerline between the two patches. In those regions, the growth of new vegetation is inhibited (Bouma et al., 2007). This self-organizing nature of the patches is however vulnerable to change. According to research by Schwarz et al. (2018), such a self-organizing landscape can change to either a fully vegetated or bare landscape due to a change in certain factors. For example, if the morphological development in a river accelerates, a self-organizing landscape could turn into a bare landscape (Schwarz et al., 2018). It is thus important to keep in mind that there are other factors that can have a large influence on vegetation growth, other than the self-organizing nature of the patches themselves. These factors are hard to predict, which makes it difficult to make a definitive statement about the evolution and growth of vegetation.

6 Conclusion

As river vegetation both has a lot of positive effects on the environment, but also some negative, it is important to understand more of its influence on the flow. This study focuses on two neighbouring vegetation patches with each a different density, and how that plays a role in the distribution of flow velocity and turbulence in the study domain. The conclusion of this study is built up in the following order. First, the three sub questions will be answered individually, which help to then formulate an answer to the research objective and general research question.

1. Which model settings and turbulence closure model is the most successful in achieving realistic values for the flow velocity and turbulent kinetic energy compared to results from literature?

The patch shape that generates the best correspondence to the validation data is the circular patch with 37 stems. Different initial conditions barely have an effect on the simulation, which is why the standard values are chosen. This means an inlet velocity of 0.098 m/s and a turbulence intensity of 5%. From the model validation it becomes clear that the RNG $k-\epsilon$ model with standard wall functions proves most suitable in this case. With this patch type and model settings, the error between the experimental and simulated flow velocities is the lowest (11%), and the simulated steady wake length shows a decent agreement with the steady wake length behind the validation patch. The difference between these lengths is $1D$. However, the many differences between the use of different models and wall functions highlights the need for model validation, as no model can be trusted to be universally best.

2. What is the effect of changing the density of each patch and altering the interpatch distance on the flow recovery pattern and length for the whole horizontal domain?

Changing the density of the downstream patch has a significant effect on the steady wake length of the upstream patch when the patches are placed at L=$4D$. Due to the flow diversion around the downstream patch, the wake of the upstream patch is shortened. The density of this downstream patch does have an effect on the shortening of the steady wake length of the upstream patch. A denser downstream patch results in a shorter wake length and a sparser patch results in a longer wake length, however these lengths are always shorter than the wake length behind an individual patch. For a denser downstream patch, the minimum velocity in the wake is also higher as the the downstream patch interferes before the wake of the upstream patch reaches this minimum velocity.

The steady wake length behind an upstream patch that is placed L=$6D$ away from its downstream neighbour is not as much affected. This is because the steady wake length of an individual patch is around $5D$, which means that the downstream patch only interferes with the wake of the upstream patch after the steady wake region has ended. However, the recovery of a wake in the presence of a downstream patch is still very different from the flow recovery behind an individual patch. At the end of the steady wake region, enhanced velocities on the sides of the downstream patch mix with the wake of the upstream patch, resulting in a rapid rise of the flow velocity. This is also the case for patches placed at L=$4D$ from each other. For denser downstream patches, this rise is faster than for the sparser downstream patches.

When the patches are placed at T=$1.3D$, the velocity reaches a peak almost equal to or above the undisturbed upstream velocity for the two densest downstream patches (ϕ=14 and 19%). Afterwards, the velocity drops a little as the patch wakes start to merge. For patches placed at T=$2.5D$, this peak does not occur, although the recovery to the upstream undisturbed flow velocity is much faster than for patches placed at T=$1.3D$. Because the patches are placed so far from each other, the wakes of each patch mix with the jet stream and merge much further downstream.

The TKE profiles follow the same pattern as the velocity profiles. A denser downstream patch results in a higher TKE peak at the end of the steady wake region behind the upstream patch. This is a result of the steeper velocity gradient caused by higher velocities diverting around a denser downstream patch. This is also reflected in the transverse longitudinal velocity profiles, where a steeper velocity gradient is visible for patch combinations with a higher density. The TKE peak is also placed further upstream for a denser downstream patch, as a larger part of the flow is diverted around this patch and therefore mixes faster with the upstream wake. A highest TKE peak is generated by the patches placed at a distance of L=6D, caused by a high velocity gradient between the jet stream and the low steady wake velocity.

The wake behind downstream patches is not affected much by a different upstream density. The most significant effect is observed upstream of the downstream patch, where the flow diverted around the upstream patch increases the flow velocity that approaches the downstream patch. The increased velocities on the sides of the downstream patch result in steep velocity gradients, as also shown by the transverse velocity plots. The steep velocity gradients elevate the turbulence levels. For denser upstream patches, these velocity gradients are steeper which results in higher turbulence levels. As the steady wake lengths behind the downstream patch are similar for different upstream patch densities, the TKE peak does not vary in location.

3. How is sediment deposition and vegetation growth affected by changing the density for each patch and the interpatch distance?

Regions of potential new vegetation growth are assessed by the occurrence of enhanced sediment deposition. When enhanced sediment deposition takes place, plant propagules can settle down as well, which grow into new vegetation patches. Two different methods have been tested to provide an answer to this research question. Both methods found that the total flow blockage presented by the two patches had an influence on the area of enhanced sediment deposition and consequently the potential for new vegetation growth.

With the method that takes the influence of TKE into account, the conclusion is drawn that the presence of sparser patches results in a larger area of enhanced sediment deposition. Placing two patches at different locations (L=4D and T=1.3D, L=4D and T=2.5D, L=6D and T=1.3D) has no influence on the area of enhanced sediment deposition, as long as the combined flow blockage generated by the two patches stays the same. The method that uses a threshold velocity to assess sediment deposition results in the opposite effect: the presence of denser patches generates a larger area of enhanced sediment deposition. Increasing the longitudinal distance between the upstream and downstream patch from L=4D to L=6D leads to a small increase in the size of the area for potential vegetation growth, however this difference is small in comparison to the increase in area generated by increasing the patch density. In two specific instances, enhanced sediment deposition and consequently vegetation growth was also promoted by placing either the sparsest (ϕ=3%) and the densest (ϕ=19%) patch 4D upstream of a patch of more medium density (ϕ=10%) instead of downstream.

With these three sub questions the main research question of this study can be answered:

What is the effect of vegetation patches with different densities on the flow velocity distribution and sediment deposition?

Changing the density of the upstream patch does not have a large effect on the wake velocity of the downstream patch. The turbulence levels in the wake of the downstream patch are affected and become higher for a denser upstream patch. Changing the density of a downstream patch does have a large effect on the flow velocity and turbulence in the wake of the upstream patch. For all

interpatch distances tested in this research, the influence of the density of a downstream patch had the same effects. For a denser downstream patch, the steady wake length behind the upstream patch shortens and has a higher velocity. Turbulence levels are higher and a turbulence peak is found further upstream than in the case of a sparser downstream patch. This is similar when the patches are placed further apart in the transverse direction. When patches are placed further apart in the longitudinal direction, the influence of a downstream patch of different density is not as significant in the steady wake behind the upstream patch, however in this scenario the largest TKE peaks are found, related to the steep velocity gradients. From the velocity and TKE method for measuring enhanced sediment deposition, it can be concluded that the distance between the patches does not have an effect on the total area of enhanced sediment deposition. According to this method, patch pairs with a sparser patch generate a larger area for enhanced sediment deposition and thus potential new vegetation growth. The velocity threshold method states that patch pairs with a denser patch will generate a larger area of enhanced sediment deposition. According to this method, the position of the upstream and downstream patch do matter, in which the potential area for new vegetation growth becomes larger when either the most sparse (ϕ=3%) or the most dense (ϕ=19%) are placed upstream. Overall, for both methods, the amount of new vegetation growth is more dependent on the density of the two patches than the varying interpatch distances. Sediment deposition is most present downstream of each patch, meaning that the patches can expand in the longitudinal direction. Patch merger is not likely, as for the tested interpatch distances, no secondary deposition zone is found.

7 Recommendations

7.1 Model optimization and practical application

This section elaborates on some recommendations to improve the model performance. Furthermore, some recommendations for the practical application of this research are made.

- When setting up the model and choosing the model domain, perform runs with all different patch shapes and densities in order to find dimensions that suit all. Using a model domain that is too small can have an impact on the results, as it limits the model in predicting values that are close to a real-life scenario.
- The discussion in Section 5 dives into the many uncertainties related to RANS numerical modelling. Due to these uncertainties, the reliability of the simulated flow velocity and TKE values are questionable. This is one of the main reasons why this research does not go as much into actual numbers of the flow velocity or steady wake length, but much rather compares different scenarios against each other in order to make a general statement. On the other hand, as mentioned throughout the results section (Section 4.2), the shape and pattern of the velocity and TKE profiles is often in line with experimental findings. For practical application, this means that this research could mainly be useful to extract the observed patterns and general behaviour associated with varying patch densities and varying interpatch distances.
- This research can be used as additional information to support river management. The information presented in this research can be used to gain a general idea of the interaction between two vegetation patches of different densities. It could be used as a tool to predict new vegetation growth, but also to analyse the change in flow velocity and turbulence in a river when a second patch starts growing. When new vegetation growth is of interest, this research provides some additional information on the self-organizing nature of vegetation and how it can be used to optimize vegetation growth.

7.2 Future research

This section elaborates on some recommendations for future research related to this study, in order to get a better grip on all processes related to river-based vegetation patches.

- Initially, the wake behind a downstream patch seems less interesting because the density of an upstream patch hardly affects the velocity in the downstream patch wake, and although the TKE peak is larger for a denser upstream patch, the shape of the profile remains the same throughout various runs. However, it would be interesting to investigate if the relation between the increased velocity in front of the downstream patch and the increased TKE behind the downstream patch also holds for different distances. Due to limited time and model complications, these runs were not performed, but these are compelling scenarios for further research.
- More research is needed into a method that accurately describes the location where enhanced sediment deposition takes place. A good start has been made to connect areas of low flow velocities to regions where the TKE is also low, however more experimental analysis in this study area is needed to get a good grip on how to apply it in numerical models as well. An addition to this could be that the numerical model used to model this could be a LES model which is more capable at calculating the finer areas of turbulence close to the vegetation patch.
- Up to this point, not much research has focused on investigating the solid volume fractions related to (representative) species of emergent vegetation. The selected densities of the simulated vegetation patches in this research are based on a selection made by many other researches,

such as Kitsikoudis et al. (2020), Zong and Nepf (2012), de Lima et al. (2015) and Meire et al. (2014). The choice they make for their range of densities is often not related to the characteristics of specific vegetation species, but has more to do with the behaviour of flow around a patch of specific density. Zong and Nepf (2010) state that channel vegetation usually has a solid volume fraction between 0.5% and 10%. A solid volume fraction above 10% is usually associated with mangroves, although these claims are not verified by any other sources. From field observations, Kibler et al. (2019) found a solid volume fraction of 7% for an area covered with mangrove forest. In order to apply this research and work with the evaluated densities, it is important that more research is conducted into what range of solid volume fractions are related to which species of vegetation.

8 Bibliography

ANSYS Inc (2009a) Ansys fluent 12.0 theory guide - 18. solver theory. URL https://www.afs.enea.it/project/neptunius/docs/fluent/html/th/node359.htm, last accessed 31 May 2022

ANSYS Inc (2009b) Ansys fluent 12.0 user's guide. URL https://www.afs.enea.it/project/neptunius/docs/fluent/html/ug/main_pre.htm, last accessed 31 May 2022

ANSYS Inc (2010) Ansys fluent 13.0 release - lecture 5: Solver settings. URL https://imechanica.org/files/fluent_13.0_lecture05-solver-settings.pdf, last accessed 31 May 2022

ANSYS Inc (2014) Ansys fluent 15.0 release - lecture 7: Turbulence modeling. URL https://www.researchgate.net/profile/Subhasisa-Rath/post/How-to-select-the-wall-function-in-the-process-of-using-ANSYS-fluent-And-is-there-any-some-priciples-to-guide-for-the-user/attachment/5b90f3b63843b0067538096e/AS%3A667795364798465%401536226230381/download/FluentIntro_15.0_L07_Turbulence.pdf, last accessed 19 April 2022

Bardina J, Huang P, Coakley T (1997) Turbulence modeling validation, testing, and development. *NASA Technical Memorandum*

Bouma T, van Duren L, Temmerman S, Claverie T, Blanco-Garcia A, Ysebaert T, Herman P (2007) Spatial flow and sedimentation patterns within patches of epibenthic structures: Combining field, flume and modelling experiments. *Continental Shelf Research* 27(8):1020–1045, DOI https://doi.org/10.1016/j.csr.2005.12.019, natural Coastal Mechanisms - Flume and Field Experiments on Links between Biology, Sediments and Flow

Chang K, Constantinescu G (2015) Numerical investigation of flow and turbulence structure through and around a circular array of rigid cylinders. *Journal of Fluid Mechanics* 776:161–199, DOI 10.1017/jfm.2015.321

Chen Z, Ortiz A, Zong L, Nepf H (2012) The wake structure behind a porous obstruction and its implications for deposition near a finite patch of emergent vegetation. *Water Resources Research* 48(9):9517–, DOI 10.1029/2012WR012224

Cornacchia L, Licci S, Nepf H, van der Wal D, Folkard A, van de Koppel J, Puijalon S, Bouma T (2019) Turbulence-mediated facilitation of resource uptake in patchy stream macrophytes. *Limnology and oceanography* 64(2):714–727, DOI 10.1002/lno.11070, https://aslopubs.onlinelibrary.wiley.com/doi/epdf/10.1002/lno.11070

Costanza R, d'Arge R, Groot R, Farber S, Grasso M, Hannon G, Limburg K, Naeem S, O'Neill R, Paruelo J, Raskin R, Sutton P, Belt M, Belt H (1996) The value of the world's ecosystem services and natural capital. *Nature* 387:253–260, DOI 10.1038/387253a0

Durbin P (2004) Turbulence Closure Models for Computational Fluid Dynamics, vol 3. DOI 10.1002/0470091355.ecm061

Fröhlich J, von Terzi D (2008) Hybrid les/rans methods for the simulation of turbulent flows. *Progress in Aerospace Sciences* 44(5):349–377, DOI https://doi.org/10.1016/j.paerosci.2008.05.001

Giraldo G (2021) Cfd modeling, analysis, and online simulation for beginners. Simscale, URL https://www.simscale.com/blog/2019/04/cfd-analysis-for-beginners/, last accessed 20 Januari 2022

Gurnell A (2014) Plants as river system engineers. *Earth Surface Processes and Landforms* 39(1):4–25, DOI https://doi.org/10.1002/esp.3397

Jones DA, Chapuis M, Liefvendahl M, Norrison D, Widjaja R (2016) Rans simulations using openfoam software. Australian government, department of defence

Jones JI, Collins A, Naden P, Sear DA (2012) The relationship between fine sediment and macrophytes in rivers. *River Research and Applications* 28:1006–1018, DOI 10.1002/rra.1486

Kemp J, Harper D, Crosa G (2000) The habitat-scale ecohydraulics of rivers. *Ecological Engineering - ECOL ENG* 16:17–29, DOI 10.1016/S0925-8574(00)00073-2

Kibler KM, Kitsikoudis V, Donnelly M, Spiering DW, Walters L (2019) Flow–vegetation interaction in a living shoreline restoration and potential effect to mangrove recruitment. *Sustainability* 11(11), DOI 10.3390/su11113215, URL https://www.mdpi.com/2071-1050/11/11/3215

Kitsikoudis V, Huthoff F (2021) River flow processes, lecture notes. Water Engineering and Management, Department of Civil Engineering, Faculty of Engineering Technology, University of Twente

Kitsikoudis V, Yagci O, Ozgur Kirca V (2020) Experimental analysis of flow and turbulence in the wake of neighboring emergent vegetation patches with different densities. *Environmental Fluid Mechanics* 20:1417–1439, DOI 10.1007/s10652-020-09746-6

Kondziolka J, Nepf H (2014) Vegetation wakes and wake interaction shaping aquatic landscape evolution. *Limnology Oceanography: Fluids Environments* 4:106–119, DOI 10.1215/21573689-2846314

Langtry RB, Menter FR (2009) Correlation-based transition modeling for unstructured parallelized computational fluid dynamics codes. *AIAA Journal* 47(12):2894–2906, DOI 10.2514/1.42362, https://doi.org/10.2514/1.42362

de Lima PH, Janzen JG, Nepf HM (2015) Flow patterns around two neighboring patches of emergent vegetation and possible implications for deposition and vegetation growth. *Environmental Fluid Mechanics* 15:881–898, DOI 10.1007/s10652-015-9395-2

Mcquivey RS (1973) Summary of turbulence data from rivers, conveyance channels, and laboratory flumes. US Geological Survey, vol 802, DOI 10.3133/pp802b

Meire D, Kondziolka J, Nepf H (2014) Interaction between neighboring vegetation patches: Impact on flow and deposition. *Water Resources Research* 50:3809– 3825, DOI 10.1002/2013WR015070

Nepf HM (2012) Hydrodynamics of vegetated channels. *Journal of Hydraulic Research* 50:262–279, DOI 10.1080/00221686.2012.696559

Ortiz AC, Ashton A, Nepf HM (2013) Mean and turbulent velocity fields near rigid and flexible plants and the implications for deposition. *Journal of Geophysical Research: Earth Surface* 118(4):2585–2599, DOI https://doi.org/10.1002/2013JF002858

ten Pas S (2016) The influence of y+ in wall functions applied in ship viscous flows. Dept. of Engineering Technology, University of Twente, URL https://essay.utwente.nl/69529/1/MARIN%20-%20S.%20ten%20Pas%20Internship.pdf, internship report for MARIN

Rapp BE (2017) Chapter 9 - fluids. In: Rapp BE (ed) Microfluidics: Modelling, Mechanics and Mathematics, Micro and Nano Technologies, Elsevier, Oxford, pp 243–263, DOI https://doi.org/10.1016/B978-1-4557-3141-1.50009-5

Rominger JT, Nepf HM (2011) Flow adjustment and interior flow associated with a rectangular porous obstruction. *Journal of Fluid Mechanics* 680:636–659, DOI 10.1017/jfm.2011.199

Schnauder I, Moggridge H (2009) Vegetation and hydraulic-morphological interactions at the individual plant. *Aquatic Sciences* 71:318–330, DOI 10.1007/s00027-009-9202-6

Schwarz C, Gourgue O, van Belzen J, Zhu Z, Bouma T, van de Koppel J, Ruessink G, Claude N, Temmerman S (2018) Self-organization of a biogeomorphic landscape controlled by plant life-history traits. *Nature geoscience* 11(9):672–677, DOI 10.1038/s41561-018-0180-y

Stankovic B, Stojanovic A, Sijercic M, Belosevic S, Cantrak S (2014) Evaluation and limitations of standard wall functions in channel and step flow configurations. *Journal of the Serbian Society for Computational Mechanics* 8:1–22, DOI 10.5937/jsscm1401001S

Vandenbruwaene W, Temmerman S, Bouma T, Klaassen P, de Vries M, Callaghan D, van Steeg P, Dekker F, van Duren L, Martini E, Balke T, Biermans G, Schoelynck J, Meire P (2011) Flow interaction with dynamic vegetation patches: implications for biogeomorphic evolution of a tidal landscape. *Journal of geophysical research* 116, DOI 10.1029/2010JF001788

Yagci O, Yildirim I, Celik MF, Kitsikoudis V, Duran Z, Kirca VSO (2017) Clear water scour around a finite array of cylinders. *Applied Ocean Research* 68:114–129

Yamasaki T, de Lima PHS, Silva DF, de A Preza CG, Janzen JG, Nepf HM (2019) From patch to channel scale: The evolution of emergent vegetation in a channel. *Advances in Water Resources* 129:131–145

Yamasaki T, Jiang B, Janzen JG, Nepf HM (2021) Feedback between vegetation, flow, and deposition: A study of artificial vegetation patch development. *Journal of Hydrology* 598

Ye W, Pan Y, He L, Chen B, Liu J, Gao J, Wang Y, Yang Y (2021) Chapter 3 - design with modeling techniques. In: Goodfellow HD, Wang Y (eds) Industrial Ventilation Design Guidebook (Second Edition), second edition edn, Academic Press, pp 109–183, DOI https://doi.org/10.1016/B978-0-12-816673-4.00008-0

Zong L, Nepf H (2010) Flow and deposition in and around a finite patch of vegetation. *Geomorphology* 116(3):363–372, DOI https://doi.org/10.1016/j.geomorph.2009.11.020, geomorphology and Vegetation: Interactions, Dependencies, and Feedback Loops

Zong L, Nepf HM (2011) Spatial distribution of deposition within a patch of vegetation. *Water Resources Research* 47(3), DOI 10.1029/2010WR009516

Zong L, Nepf HM (2012) Vortex development behind a finite porous obstruction in a channel. *Journal of Fluid Mechanics* 691:368–391, DOI 10.1017/jfm.2011.479

A Model specifications

This section elaborates on the methods that were selected as input for the simulation runs. As a solver, the SIMPLE solver was chosen which is a steady-state solver. Then the following spatial discretization schemes were used:

- Gradient: Least squares cell based
- Pressure: Second order scheme
- Momentum: Second order upwind
- Turbulent Kinetic Energy: Second order upwind
- Turbulent dissipiation rate: Second order upwind

Residuals for the continuity, x-velocity, y-velocity, k and epsilon were all set to 10^{-6}.

B Additional plots and figures

B.1 Velocity distribution for two staggered patches

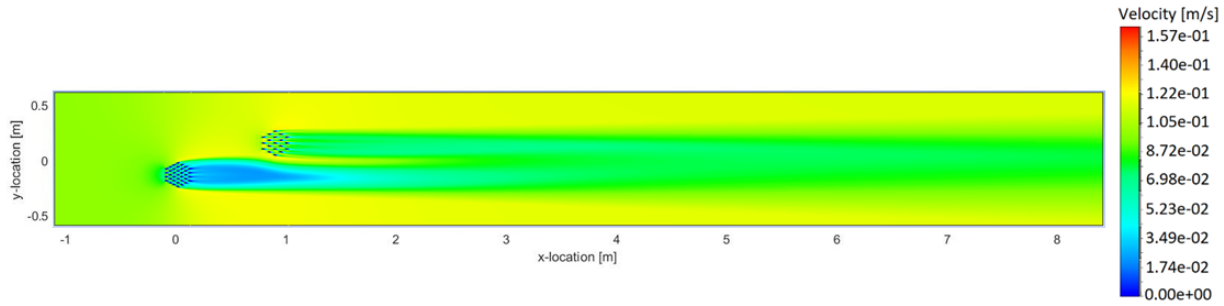

Figure B.1: Distribution of velocities throughout the model domain for an upstream patch of ϕ=10% and a downstream patch of ϕ=3%. The distances between the patches are T=1.3D and L=4D.

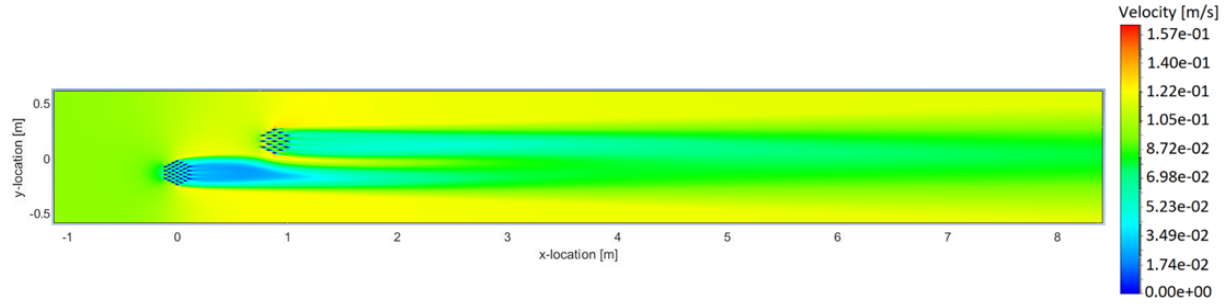

Figure B.2: Distribution of velocities throughout the model domain for an upstream patch of ϕ=10% and a downstream patch of ϕ=6%. The distances between the patches are T=1.3D and L=4D.

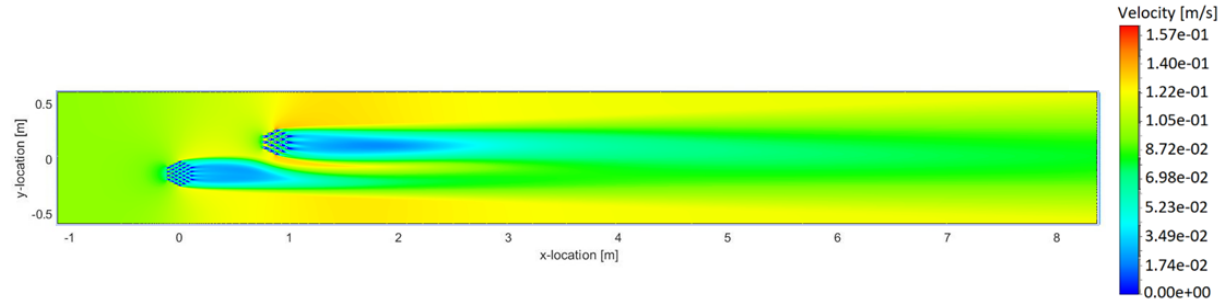

Figure B.3: Distribution of velocities throughout the model domain for an upstream patch of ϕ=10% and a downstream patch of ϕ=14%. The distances between the patches are T=1.3D and L=4D.

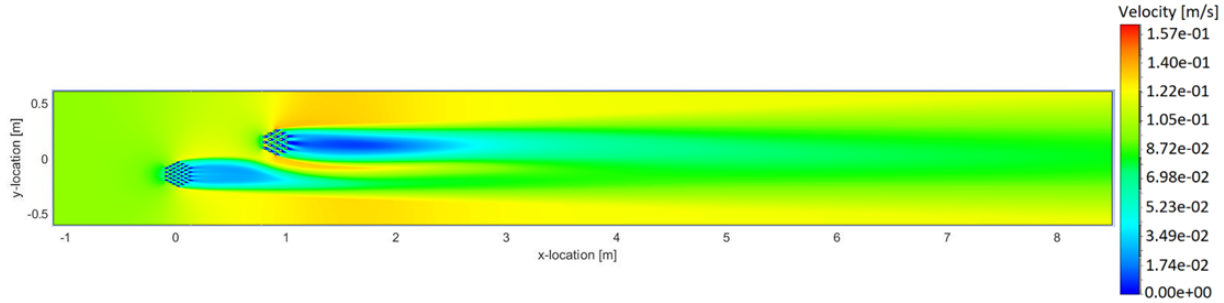

Figure B.4: Distribution of velocities throughout the model domain for an upstream patch of ϕ=10% and a downstream patch of ϕ=19%. The distances between the patches are T=1.3D and L=4D.

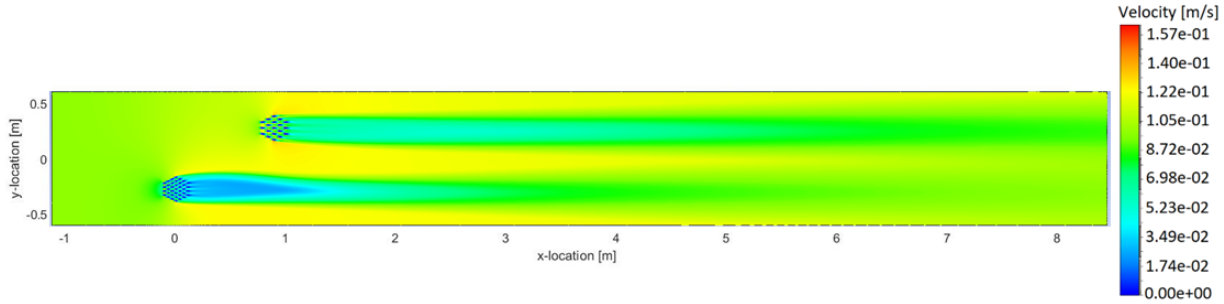

Figure B.5: Distribution of velocities throughout the model domain for an upstream patch of ϕ=10% and a downstream patch of ϕ=6%. The distances between the patches are T=2.5D and L=4D.

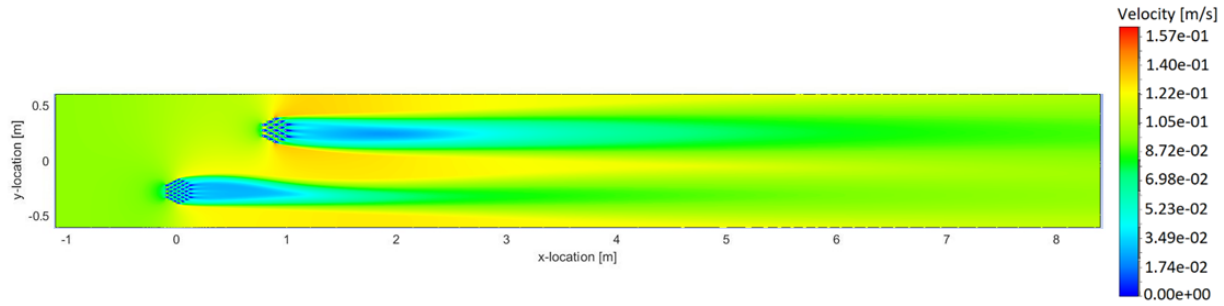

Figure B.6: Distribution of velocities throughout the model domain for an upstream patch of ϕ=10% and a downstream patch of ϕ=14%. The distances between the patches are T=2.5D and L=4D.

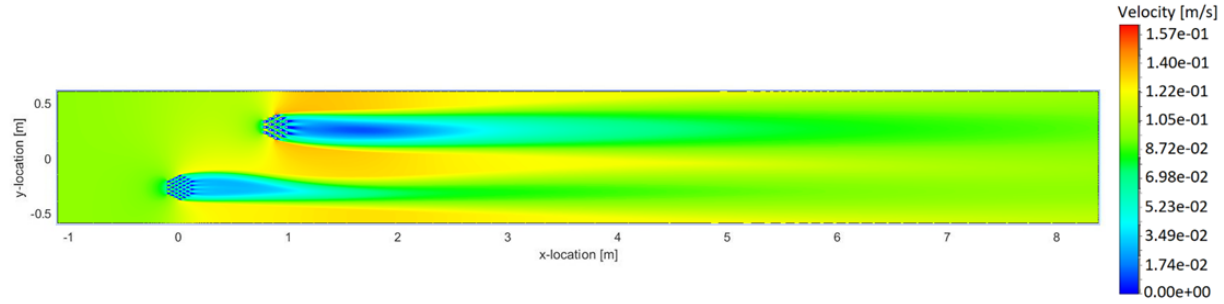

Figure B.7: Distribution of velocities throughout the model domain for an upstream patch of ϕ=10% and a downstream patch of ϕ=19%. The distances between the patches are T=2.5D and L=4D.

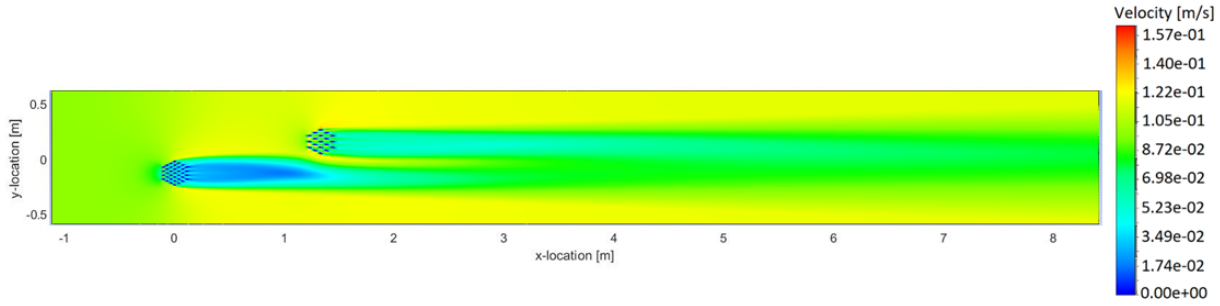

Figure B.8: Distribution of velocities throughout the model domain for an upstream patch of ϕ=10% and a downstream patch of ϕ=6%. The distances between the patches are T=1.3D and L=6D.

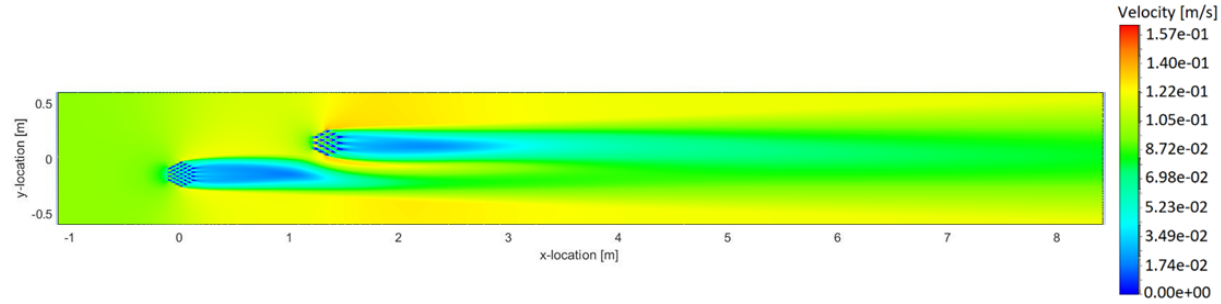

Figure B.9: Distribution of velocities throughout the model domain for an upstream patch of ϕ=10% and a downstream patch of ϕ=14%. The distances between the patches are T=1.3D and L=6D.

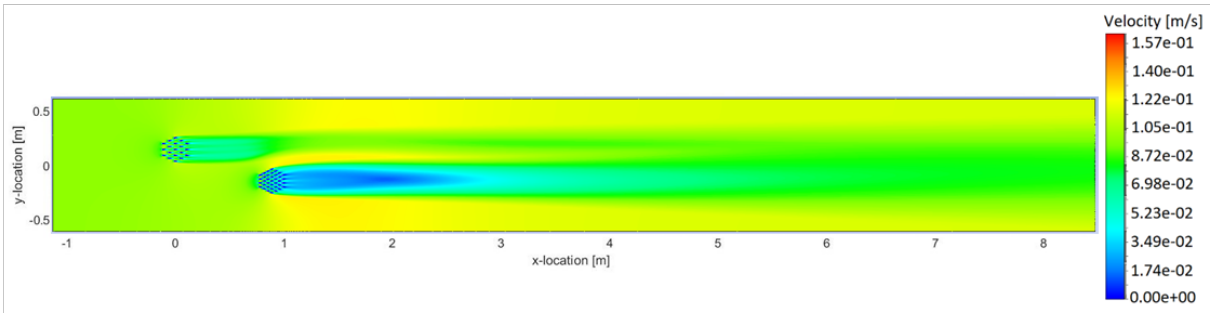

Figure B.10: Distribution of velocities throughout the model domain for an upstream patch of ϕ=3% and a downstream patch of ϕ=10%. The distances between the patches are T=1.3D and L=4D.

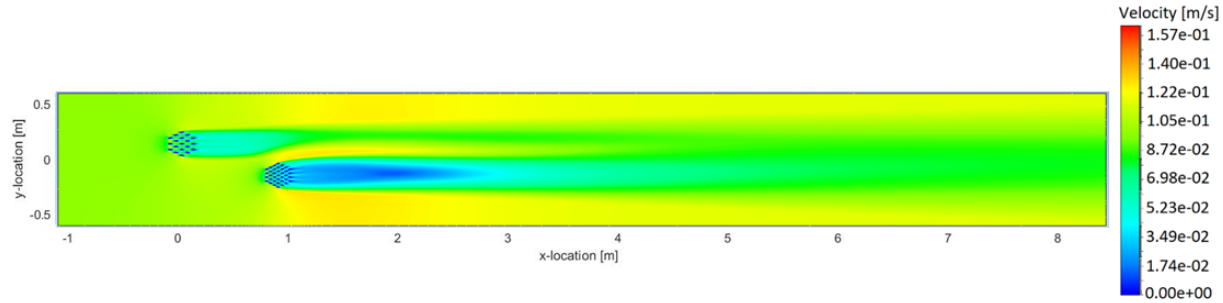

Figure B.11: Distribution of velocities throughout the model domain for an upstream patch of ϕ=6% and a downstream patch of ϕ=10%. The distances between the patches are T=1.3D and L=4D.

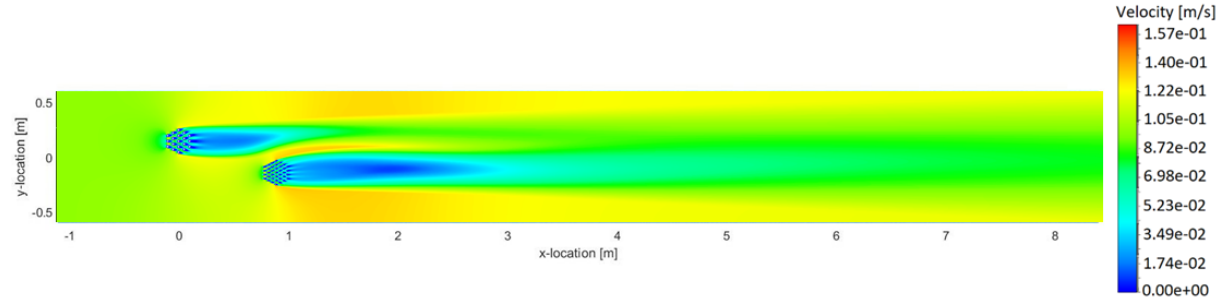

Figure B.12: Distribution of velocities throughout the model domain for an upstream patch of ϕ=19% and a downstream patch of ϕ=10%. The distances between the patches are T=1.3D and L=4D.

B.2 Enhanced sediment deposition profiles for two staggered patches

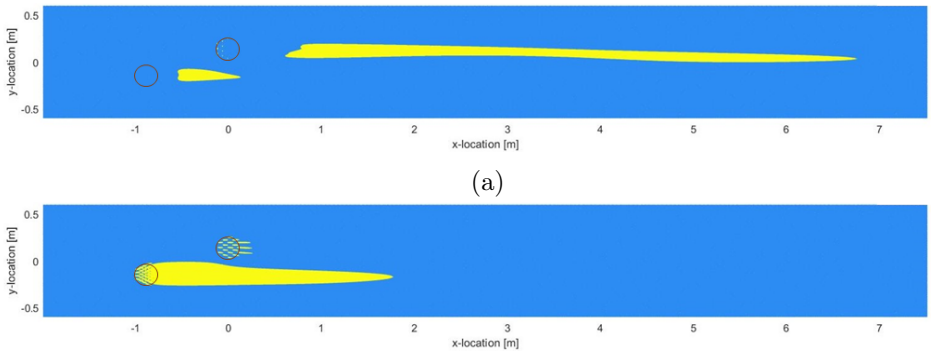

(a)

(b)

Figure B.13: Sediment deposition according to the velocity and TKE method (a) and the velocity threshold method (b) for Run 1. The yellow areas signify the location of enhanced sediment deposition. The blue areas signify the rest of the model domain. The red circles represent the outlines of the vegetation patches.

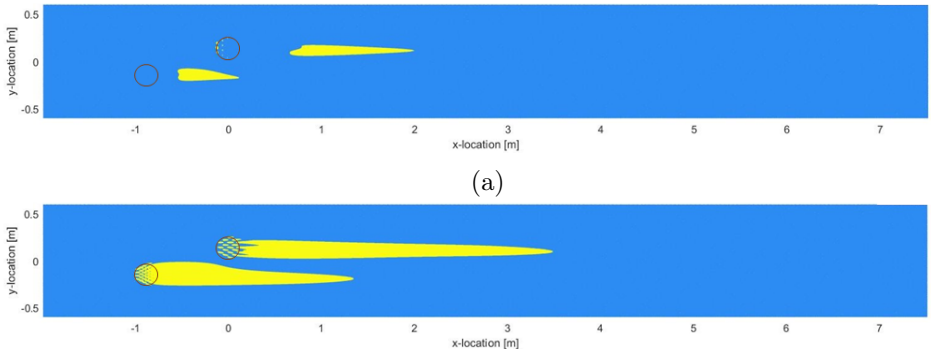

(a)

(b)

Figure B.14: Sediment deposition according to the velocity and TKE method (a) and the velocity threshold method (b) for Run 2. The yellow areas signify the location of enhanced sediment deposition. The blue areas signify the rest of the model domain. The red circles represent the outlines of the vegetation patches.

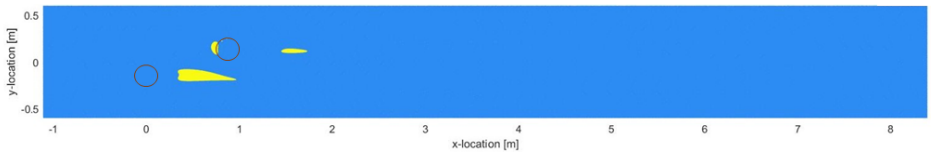

(a)

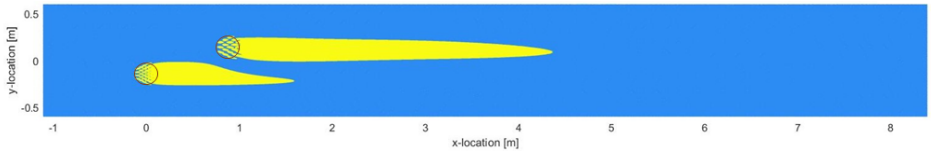

(b)

Figure B.15: Sediment deposition according to the velocity and TKE method (a) and the velocity threshold method (b) for Run 5. The yellow areas signify the location of enhanced sediment deposition. The blue areas signify the rest of the model domain. The red circles represent the outlines of the vegetation patches.

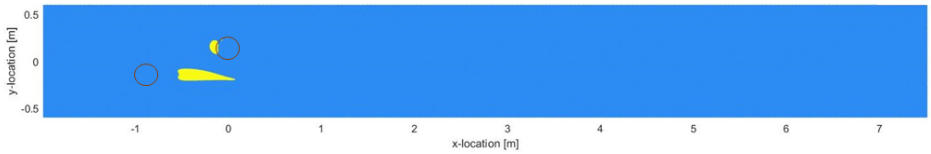

(a)

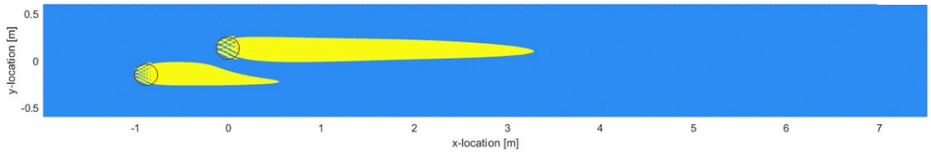

(b)

Figure B.16: Sediment deposition according to the velocity and TKE method (a) and the velocity threshold method (b) for Run 6. The yellow areas signify the location of enhanced sediment deposition. The blue areas signify the rest of the model domain. The red circles represent the outlines of the vegetation patches.

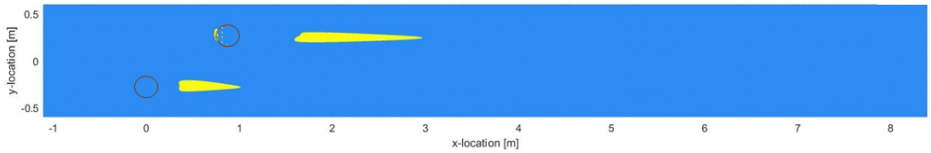

(a)

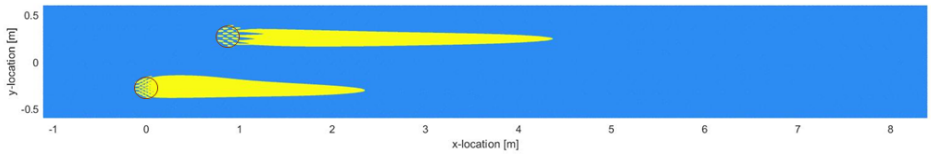

(b)

Figure B.17: Sediment deposition according to the velocity and TKE method (a) and the velocity threshold method (b) for Run 7. The yellow areas signify the location of enhanced sediment deposition. The blue areas signify the rest of the model domain. The red circles represent the outlines of the vegetation patches.

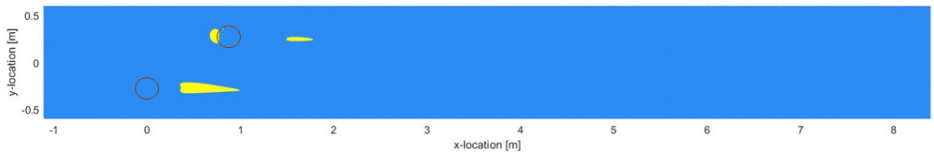

(a)

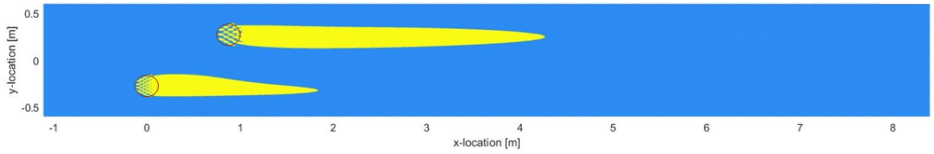

(b)

Figure B.18: Sediment deposition according to the velocity and TKE method (a) and the velocity threshold method (b) for Run 8. The yellow areas signify the location of enhanced sediment deposition. The blue areas signify the rest of the model domain. The red circles represent the outlines of the vegetation patches.

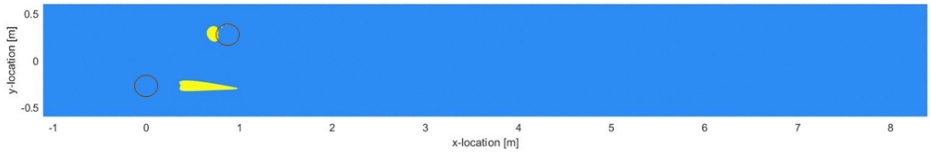

(a)

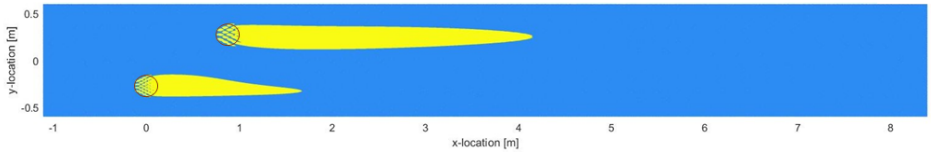

(b)

Figure B.19: Sediment deposition according to the velocity and TKE method (a) and the velocity threshold method (b) for Run 9. The yellow areas signify the location of enhanced sediment deposition. The blue areas signify the rest of the model domain. The red circles represent the outlines of the vegetation patches.

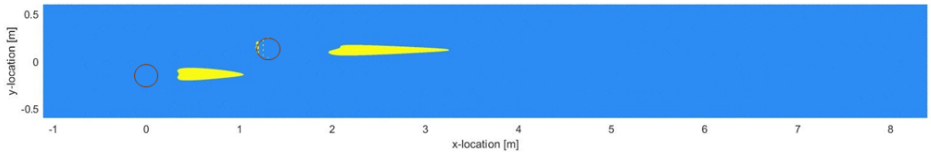

(a)

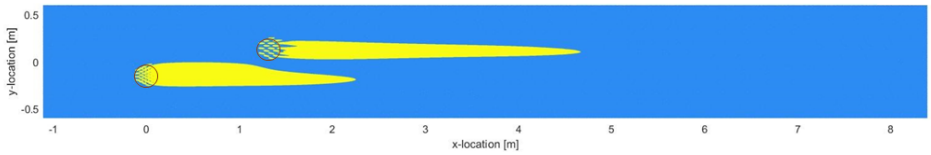

(b)

Figure B.20: Sediment deposition according to the velocity and TKE method (a) and the velocity threshold method (b) for Run 10. The yellow areas signify the location of enhanced sediment deposition. The blue areas signify the rest of the model domain. The red circles represent the outlines of the vegetation patches.

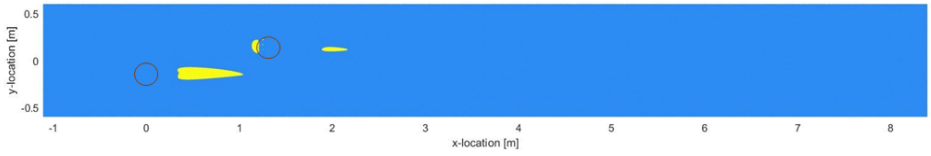

(a)

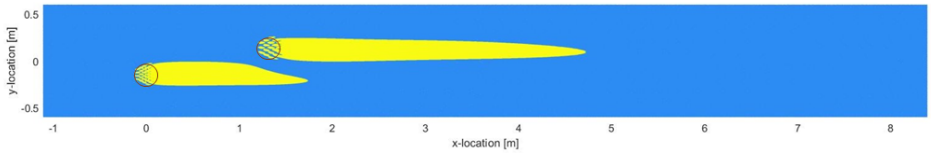

(b)

Figure B.21: Sediment deposition according to the velocity and TKE method (a) and the velocity threshold method (b) for Run 11. The yellow areas signify the location of enhanced sediment deposition. The blue areas signify the rest of the model domain. The red circles represent the outlines of the vegetation patches.

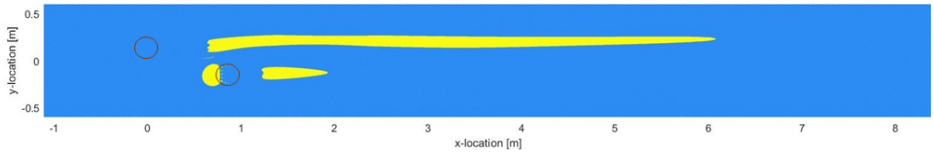

(a)

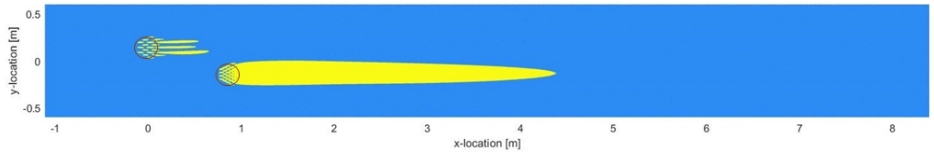

(b)

Figure B.22: Sediment deposition according to the velocity and TKE method (a) and the velocity threshold method (b) for Run 12. The yellow areas signify the location of enhanced sediment deposition. The blue areas signify the rest of the model domain. The red circles represent the outlines of the vegetation patches.

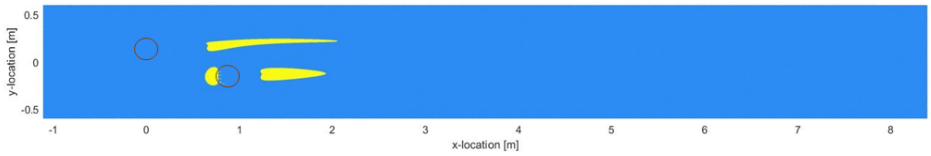

(a)

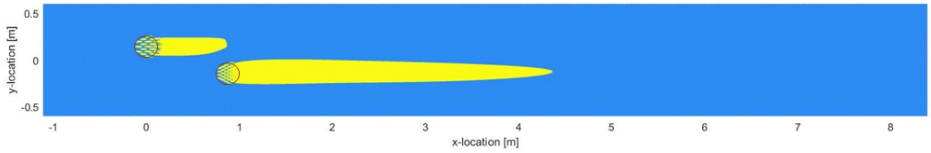

(b)

Figure B.23: Sediment deposition according to the velocity and TKE method (a) and the velocity threshold method (b) for Run 13. The yellow areas signify the location of enhanced sediment deposition. The blue areas signify the rest of the model domain. The red circles represent the outlines of the vegetation patches.

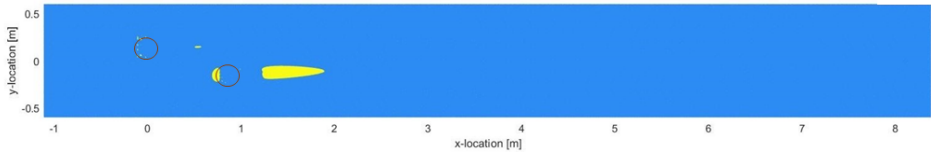

(a)

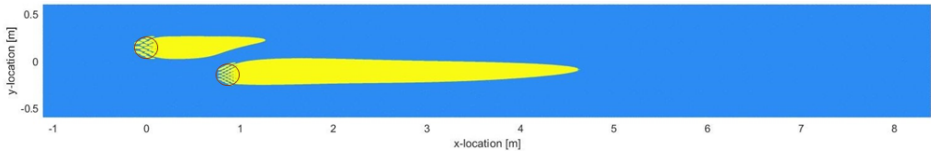

(b)

Figure B.24: Sediment deposition according to the velocity and TKE method (a) and the velocity threshold method (b) for Run 14. The yellow areas signify the location of enhanced sediment deposition. The blue areas signify the rest of the model domain. The red circles represent the outlines of the vegetation patches.

B.3 Reference case

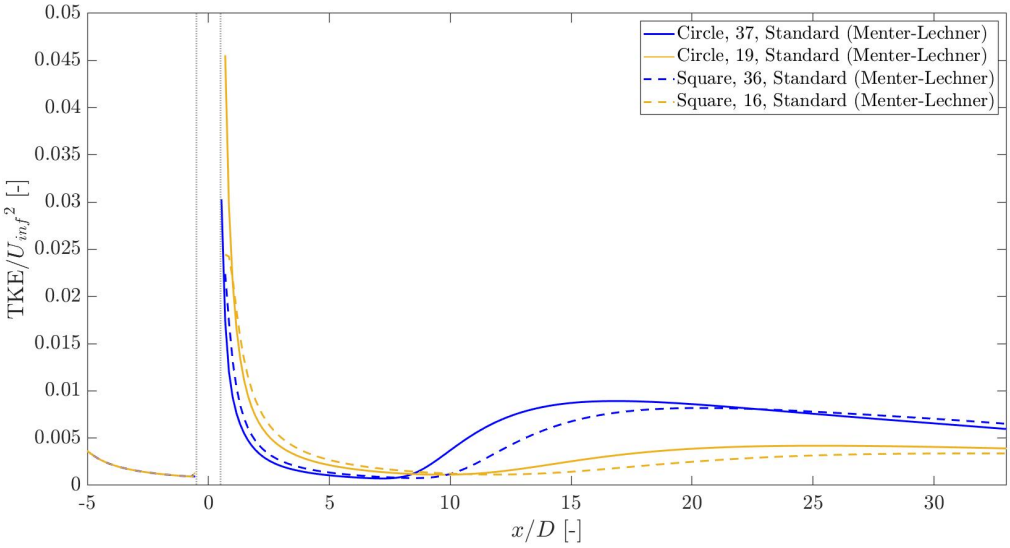

Figure B.25: Normalized TKE profiles for different patch shapes in the reference case. These runs are performed with the standard $k-\epsilon$ turbulence closure model and Menter-Lechner wall functions.